

# Accurate Extra-Galactic Distances and Dark Energy: Anchoring the Distance Scale with Rotational Parallaxes

Rob P. Olling<sup>1\*</sup>

<sup>1</sup>*Astronomy Department, University of Maryland, College Park, MD 20742-2421*

7 February 2020

## ABSTRACT

We investigate how the current and future uncertainty on the Hubble constant affects the uncertainty in the Equation of State of Dark Energy ( $w$ ) and the total density of the Universe ( $\Omega_{tot}$ ). We start with the approximate linear relations between the cosmological parameters as presented by (Spergel *et al.* 2006), and use the standard error-propagation relations to estimate the effects of improving the Cosmic Microwave Background (CMB) parameters as well as the Hubble constant ( $H_0$ ) on our knowledge of the Equation of State (EOS) of Dark Energy. Because we do not assume a flat universe, we also estimate the attainable accuracy on  $\Omega_{tot}$  and the spatial curvature of the Universe.

In one limiting case, we assume that the constraints provided by additional data (galaxy clustering, weak lensing and so forth) do not improve significantly, while the error on the Hubble constant is decreased by a factor up to ten. The other limiting case of significantly improved additional data with current  $H_0$  errors has been investigated by the Dark Energy Task Force [DETF; Albrecht *et al.* (2006)]. For the former scenario, we find that future improvements of the determination of the CMB hardly changes the accuracy with which the EOS and  $\Omega_{tot}$  are known, *unless* the Hubble constant can be measured with an accuracy of several percent. The conclusion of the DETF is that the Hubble constant hardly matters if the additional data is sufficiently accurate. We find that a combination of moderate  $H_0$  improvements with moderately improved “other” data might significantly constrain the evolution of dark energy, but at a reduced cost.

We review in some detail several methods that might yield extra-galactic distances with errors of order of several percent, where we focus on the current and future strengths and weaknesses of the methods. Specifically we review the following: the Velocity Field method, two Maser methods, two Light Echo techniques, the Binary Star method, and the “Rotational Parallax” (RP) technique. Because these methods substantially rely on geometry rather than astrophysics, their results are quite robust.

In particular we focus on the advantages of the Rotational Parallax technique which can provide single-step, bias-free distances to Local Group galaxies. These distances can be used to improve the zero-point for other distance indicators which in turn would then be able to determine the Hubble constant to greater accuracy than they currently do. Achieving an accuracy of a few percent in the zero-point distances to M31, M33 and the LMC by the RP method requires radial velocities at the 10 km s<sup>-1</sup> level and proper motions attainable by future astrometric missions such as *SIM*, *GAIA* and *OBSS*, or by future radio observatories such as the *SKA*.

**Key words:** galaxies: distances and redshifts, Local Group — galaxies: individual (Large Magellanic Cloud, M31, M33) – cosmology: cosmological parameters, dark energy and distance scale – astrometry and celestial mechanics: astrometry

## 1 INTRODUCTION

A Key Project of the Hubble Space Telescope (*HST*) resulted in a fairly accurate determination of the Hubble constant:  $H_0 = 74 \pm 2$  (random)  $\pm 7$  (systematic)  $\text{km s}^{-1} \text{Mpc}^{-1}$  (Freedman et al. 2001). There are a number of sources of systematic error, but the largest contribution to the systematic error is due to the uncertainty in the adopted distance to the Large Magellanic Cloud ( $\pm 6.5\%$ ). Notwithstanding the systematic uncertainty, relative distances measurements to galaxies can now be made with a precision (not accuracy<sup>1</sup>) of 5-10%.

The drive towards accurate cosmological parameters is in part motivated by the connection with fundamental physics theories that might be able to predict observables such as the value of the critical energy-density of the Universe  $\rho_{crit} \equiv 3H_0^2/(8\pi G)$  [e.g., Carroll (2001); Albrecht et al. (2006) and many others]. If one assumes a flat  $\Lambda$ CDM model, then the fluctuations of the cosmic microwave background (CMB) as observed by *WMAP* imply a similar value and uncertainty of  $H_0$  [ $=73 \pm 3$ , Spergel et al. (2003, 2006); hereafter referred to as WMAP07] as the *HST* results by Freedman et al. (2001). If the flatness assumption is abandoned, *WMAP* hardly constrains  $H_0$  because the *WMAP* data constrains the actual matter density: that is to say, the product of the normalized matter density ( $\Omega_m$ ) and  $h^2$  (WMAP07, their figure 20), where  $h \equiv 100 \text{ km s}^{-1} \text{Mpc}^{-1}/H_0$ , and  $\Omega_m h^2 \equiv \omega_m$  (see §3). Obviously, one way to determine  $\Omega_m$  is to accurately determine the Hubble constant.

Another way to determine  $\Omega_m$ , the Hubble constant and other cosmological parameters is to employ “other” data sets that exhibit different dependencies on  $h$ . Such a method is preferred while the error on  $h$  is of order a factor two. The constraints from other data sets used by WMAP07 are: large-scale structure observations (galaxy redshift surveys), distant type-Ia Supernovas, Big-Bang nucleosynthesis, Sunyaev-Zel’dovich (SZ) fluctuations, Lyman- $\alpha$  forest, and gravitational lensing. However, the physical processes underlying these constraints can be more complex than those of the CMB and/or “geometric” determinations of the Hubble constant. Reliance on these additional data can potentially lead to serious biases in the derived cosmological parameters [e.g., Seljak et al. (2003); Efstathiou (2005)]. Because it is beginning to become possible to achieve highly accurate “geometric” determinations of  $H_0$ , it will soon be more profitable to use  $H_0$  as an independent constraint rather than as a to-be-fitted parameter.

Combination of WMAP and the other data sets yields strong evidence that the Universe is indeed close to being flat with a total normalized density of  $\Omega_{tot} = 0.996 \pm 1.6\%$  (see section 3 below). Different combinations of *WMAP* and

ground-based data yield the equation of state ( $w$ ) of Dark Energy (DE):  $w = -0.95 \pm 12\%$ , where the equation of state (EOS) is the ratio of pressure ( $p$ ) and density ( $\rho$ ). In this paper we explore how the uncertainties on  $\Omega_{tot}$  and  $w$  depend on the uncertainty of the Hubble constant. We develop our models for the case that  $w$  does not evolve, and that the accuracies of the other data sets do not improve. We then re-scale these models to take  $w$ -evolution and data-quality improvements into account.

We find that accurate knowledge of these parameters requires better CMB data (as provided by *PLANCK*), but also significantly smaller errors on  $H_0$  (§3). In contrast, the Dark Energy Task Force (DETF) finds that the errors on  $H_0$  hardly matter as long as the other data sets improve significantly in quality [Albrecht et al. (2006), and §§3.5]. We suggest that DETF-Stage IV Dark-Energy knowledge might be achieved with less focus on large-scale surveys of the distant Universe by incorporating a highly accurate measure of  $H_0$  obtained at earlier stages such as those provided by the “Water Maser Cosmology Project” Braatz et al. (2006) and/or independently by a rotational-parallax program §4. If that is indeed the case, substantial cost and time savings might be achieved. Of course, a locally determined  $H_0$  value also serves as a completely independent check on “traditional” CMB-based  $H_0$  determinations such as WMAP07. Also, future astrometric missions will provide accurate constraints on the minimum age of the Universe as obtained from binary stars (§5).

This paper is organized as follows. In section 2 we try to summarize the current state of the zero-point of the extra galactic distance scale, with an emphasis on methods that may be able to yield extra-galactic distances at the percent level (§§2.1). In the appendix, we work out that distance estimates based on water-masers may be biased if elliptical orbits are present in AGN disks. In section 3 we discuss our modeling procedure to estimate the errors on the equation of state of Dark Energy as a function of the errors on the Hubble constant. Section 4 describes the Rotational Parallax method in detail, where we also differentiate between the abilities between the on-going and planned astrometric missions: *GAIA*, *SIM* and *OBSS*. We discuss and summarize our results in section 5. Here we also describe other (future) astrometric constraints on cosmology.

## 2 THE EXTRA-GALACTIC DISTANCE SCALE

During the past decades significant progress has been made on the calibration of the extra-galactic distance scale, and the determination of the Hubble constant with methods such as type Ia Supernovas, the Tully-Fisher relation, surface brightness fluctuations, the Tip of the Red-Giant Branch (TRGB) and the Fundamental Plane. These distance-determination techniques are now relatively free of systematic uncertainties. However, the primary calibration of these methods comes from the period-luminosity relation for Cepheid variables.

However, the true value of zero-point of the Cepheid

<sup>1</sup> In this paper we make a distinction between precision and accuracy, in the sense that the former refers to small internal errors, while the latter indicates small external errors.

distance scale is still debated, in particular the difference between the zero-points based on Cepheids in the Large Magellanic Cloud (LMC) and those in the Milky Way [*e.g.*, Feast & Catchpole (1997); Madore & Freedman (1998); Groenewegen & Oudmaijer (2000); Di Benedetto (2002); Reid (1999)]. Of the Cepheids with *HIPPARCOS* measurements (ESA 1997), all but 2 have signal-to-noise (S/N) values less than five (Feast & Catchpole 1997), so that systematic biases (*e.g.*, Lutz-Kelker correction) are important. Thus, the calibration of the Cepheid period–luminosity relation relies on Galactic Cepheids in open clusters, and is therefore tied to main-sequence fitting for clusters calibrated to the Hyades, and the till-recently-problematic Pleiades (Soderblom et al. 2005). However, steady progress is being made in the calibration of Galactic Cepheids distances via *HST* trigonometric parallaxes [Benedict et al. (2002, 2006)] and interferometric calibration of the Baade-Wesselink method (Lane et al. 2002; Nordgren et al. 2002; Kervella et al. 2004a; Kervella et al. 2004b).

Because of uncertainties in the Galactic calibration, most extra-galactic distance scale studies have been calibrated relative to the nearby LMC. However, the metallicity of the LMC is substantially below that of those distant galaxies (and the Milky Way [MW]) that are used to calibrate the Supernova Ia distance scale onto the Cepheid distance scale [*e.g.*, Sandage et al. (2006)], while there are also strong indications that the Period-Luminosity (-Color) relation is non-linear [*e.g.*, Ngeow & Kanbur (2006); Groenewegen et al. (2004) and references therein] and dependent on metallicity [*e.g.*, Gould (1994); Sasselov et al. (1997); Kennicutt et al. (2003); Groenewegen et al. (2004); Sandage et al. (2006)]. In fact, the range in recently-published values of  $H_0$  ( $58 - 75 \text{ km s}^{-1} \text{ Mpc}^{-1}$ ) may be entirely attributable to differences in the applied metallicity corrections (Sandage et al. 2006).

Several independent methods for measuring distances are commonly applied to the LMC. These include Cepheids, the Red Clump, eclipsing binaries, SN1987A, the magnitude of the TRGB, RR Lyraes, and Miras. Unfortunately, the full range of most of the distance modulus ( $\mu_{LMC}$ ) to the LMC extends from 18.2 to 18.7 mag (Reid 1999). The wide range of moduli relative to the quoted internal errors indicates that systematic errors still dominate the determinations of the LMC distance. Alves (2004) finds that recent applications of a variety of methods seem to settle on  $\mu_{LMC} = 18.5 \pm 0.1 \text{ mag}$  (or  $H_0 = 71 \pm 10 \text{ km s}^{-1} \text{ Mpc}^{-1}$ ), which corresponds nicely with the *WMAP* value. However, it is possible that such convergence is partly related to (over-) confidence in the *WMAP* results. After all, some inconsistencies remain. For example, the K-band Red-Clump distance to the Galactic centre equals  $8.24 \pm 0.4 \text{ kpc}$  (Alves 2000) while geometric methods yield values one to two sigma smaller, or about 7.3 kpc: 1) the “expanding water maser” distance to Sgr B2 equals  $7.2 \pm 0.7 \text{ kpc}$  (Reid 1993), and 2) the bias-free “orbital parallax method” (Armstrong et al. 1992)

of stars orbiting Sgr A\* yields  $7.4 \pm 0.2 \text{ kpc}$  (Ghez, 2006, private communications).

The TRGB method (Da Costa & Armandroff 1990; Lee et al. 1993) is based on a break in the luminosity function of the “giant branch,” which is due to the maximum attainable luminosity before the helium flash [*e.g.*, Iben & Renzini (1983); Salaris & Cassisi (1997)]. The TRGB method is independent of the adopted distance to the LMC because it uses Galactic Globular Clusters (and hence RR Lyrae<sup>2</sup>) as calibrators instead. For metal-poor systems, this method has a metallicity dependence of approximately  $M_I^{TRGB} \approx -3.66 + 0.14[Fe/H]^2 + 0.48[Fe/H]^2$  (Bellazzini et al. 2001) which is fairly small for  $[Fe/H] \lesssim -0.6$ , but increases rapidly towards higher metallicities. If the metallicity can be determined independently<sup>3</sup> the random errors of the TRGB method correspond to a distance error of several percent, while the systematic error of approximately 10% is mostly due to the uncertainties in the Globular Cluster distance scale [see, for example, Mouhcine et al. (2005); Rizzi et al. (2006) for recent discussions]. Thus, the TRGB will provide accurate extra-galactic distances as long as a sufficient number of RGB stars [ $\gtrsim 50$ , *e.g.*, Madore & Freedman (1995); Makarov et al. (2006)] can be resolved, and the metallicity can be estimated accurately. However, given that galaxy-halos are often the target for TRGB programs and that these halos often have large spread in metallicity (Durrell et al. 2001; Mouhcine et al. 2005b; Mouhcine 2006), metallicity effects will be important for very accurate TRGB results. Nevertheless, a large majority of accurate galaxy distances with  $D \lesssim 12 \text{ Mpc}$  currently derives from the TRGB method (Karachentsev et al. 2006). In fact, the TRGB method may be the most robust photometric method available for distance determination in the nearby Universe.

Although it would be preferable if the first steps of the distance ladder could be avoided altogether via trigonometric parallaxes, such measurements are beyond the capability of future astrometric missions such as NASA’s *SIM* PlanetQuest<sup>4</sup> [*e.g.*, (Edberg et al. 2005)], ESA’s *GAIA*<sup>5</sup> (Perryman 2002) and the proposed *OBSS* mission (Johnston et al. 2006). The accuracy of *SIM*’s grid is expected to be about  $3.5 \mu\text{as}$ , which corresponds to a distance error of about 19% for the LMC, while for *GAIA* and *OBSS* the accuracy is coarser by a factor of two. Note that *SIM*’s status is currently unclear<sup>6</sup>. The Square Kilometer

<sup>2</sup> Bellazzini et al. (2001) employ a distance to  $\omega$  Cen based on a double-line spectroscopic binary.

<sup>3</sup> In practice, the metallicity is often estimated from the photometry.

<sup>4</sup> [http://planetquest.jpl.nasa.gov/documents/WhitePaper05ver18\\_final.pdf](http://planetquest.jpl.nasa.gov/documents/WhitePaper05ver18_final.pdf)

<sup>5</sup> <http://astro.estec.esa.nl/SA-general/Projects/GAIA/gaia.html>

<sup>6</sup> While it is “placed on hold” there is 20 – 30 M\$ (US) per year in NASA’s budget for the *SIM* mission.

Array [*SKA*<sup>7</sup>; Schilizzi (2004)] will have astrometric capabilities (Fomalont & Reid 2004; Fomalont 2005) comparable to *GAIA* and *OBSS* for those sources that have strong radio emission, and will thus not be able to measure extra-galactic parallaxes directly.

Often, many members of “standard candle” group are located within several kpc from the Sun. Most of these standard-candle methods (supernovae being an obvious exception) will be revitalized with the advent of the next generation space astrometry missions. Also, it is possible to obtain rotational parallaxes at the required accuracy required for external galaxies distance determination [Peterson & Shao (1997) and Olling & Peterson (2000, 2007), hereafter referred to as OP2000]. This is discussed in § 4 below.

### 2.0.1 “Nearby” Extra-Galactic Calibrators

A future determination of an accurate distance to a single galaxy does not amount to an accurate determination of the Hubble constant<sup>8</sup>. In most cases, the Hubble constant would need to be determined via secondary calibrators in galaxies at larger distances because typical deviations from the linear Hubble flow due to interactions with companions, groups, (super)clusters and voids do occur. For nearby galaxies, the size of these effects virtually guarantee that the measured recession velocity of the calibrator is atypical for the distance of the galaxy. If a typical deviation from the Hubble flow is, say, 200 km s<sup>-1</sup>, then a 1% accuracy of the Hubble constant would require a calibrator galaxy at redshift  $200/0.01 = 20,000$  km s<sup>-1</sup>, or about 280 Mpc to eliminate the uncertainty induced by non-linear Hubble flow.

Currently, the only galaxy with a distance error of ~5% is NGC 4258. At a distance of 7.2 Mpc (Herrnstein et al. 1999; Humphreys et al. 2005) has just begun to serve as a calibrator for secondary distance indicators: the TRGB method (Mouhcine et al. 2005) and the Cepheid Period-Luminosity-Abundance relation (Newman et al. 2001; Macri et al. 2006). However, a closer calibrator with at least comparable accuracy is preferable because secondary effects due to metallicity and so forth can be studied and corrected-for on a star-by-star basis. The LMC, M31 and M33 are the obvious targets, while the rotational parallax method is the ideal method to obtain unbiased distances [see § 4].

Alternatively, one can use a larger number of less accurate nearby calibrator galaxies. If Cepheids are used as secondary distance indicators, the resulting distance error might not decrease much below 5% due to metallicity effects as well as uncertainties in the Helium abundance and other peculiarities of individual Cepheids (I thank the referee for pointing this out).

<sup>7</sup> <http://www.skatelescope.org/>; The *SKA* is planned to be fully operational around 2020.

<sup>8</sup> I thank the referee for strongly emphasizing this point

## 2.1 “Direct” Distance Measures

Fortunately, other more direct methods that can yield reliable distances have been proposed (and applied) in the literature. These methods can be applied in either the optical and/or the radio regime. Below we review the most promising of the candidates that we have been able to identify in the literature. Some science projects require extra-galactic distances with an accuracy of 5% or 10% that will be readily attainable for a large number of galaxies may be sufficient, while other projects require the very best possible accuracy. The TRGB method might be applied for projects of the former type as soon as its zero-point has been accurately established. The review below is focussed on the latter type: methods that can deliver distance accuracies at the percent level.

### 2.1.1 Velocity Field Methods

The “Rotational Parallax” (RP) method was conceived by Peterson & Shao (1997) in the *SIM* context as an extra-galactic variant of the “orbital parallax” method. In the latter method, radial velocities and proper motions of a resolved binary system are combined to yield all the orbital parameters, as well as the distance [e.g., , Armstrong et al. (1992); Davis et al. (2005)]. In the simplest extra-galactic application, one assumes that: 1) the orbits are close to circular, 2) with deviations only due to (small) random motions, 3) the inclination can be obtained from the analysis of the radial velocity field, and 4) the dynamical centre is known from the velocity field. With these simplifying assumptions and the use of just two stars per galaxy, the systemic motion of the galaxy can be subtracted and the distance determined from the orbital model and the observed radial and proper motions. A more detailed treatment can be found in (Olling & Peterson 2000, 2007) and § 4. The trigonometric-, orbital- and rotational parallax methods rely only on geometric relations, Newton’s laws of motion (and the ability to measure accurate positions, proper motions and radial velocities). These methods are entirely independent of photometric transformations, metallicities, effective-temperature scales, pulsation theory and other uncertain properties of stars such as their interiors and their atmospheres (Kurucz 2002).

The “Velocity Gradient” method is in part geometric, and in part photometric and has been applied to open clusters and modified to work for the LMC [see Gould (2000), and references therein]. In this method, the transverse velocity of the centre-of-mass of the cluster/galaxy induces an angular difference between the kinematic and photometric major axes (about 20° for the LMC). In practice this method would require radial velocity and proper motion measurements of about 10,000 stars with accuracies better than about 10 km s<sup>-1</sup> and 150  $\mu$ as yr<sup>-1</sup>, respectively, which are easily attainable by *GAIA*. The most difficult part of this method is the determination of the photometric major-axis: this requires 0.1 mmag photometric accuracies over roughly 10 degrees as well as accurate reddening estimates (Gould

2000). Although it may not be possible to obtain such data from the ground, *GAIA* is well-equipped to deliver all the required data for this method. This method might also be applied to *GAIA* data of M 33. The high inclination of M 31 will likely preclude successful application of the velocity gradient method. Note that in practice the Rotational Parallax Method (or a simplified version thereof) may be needed to determine the systemic proper motion of the LMC [see § 4 and Olling & Peterson (2000)].

### 2.1.2 Maser Methods

Water masers associated with star forming regions scattered across the disk of a spiral galaxy can be used to estimate the distance to that galaxy. With two masers sources located on “opposite” sides of the centre, the known rotation curve and inclination of the galaxy can be used to derive the distance. Brunthaler et al. (2005) identified 37 maser features in two masing complexes in M 33 for which they could determine proper motions. From the per-complex average motion in combination with the velocity-field model, Brunthaler et al. (2005) determined the distance to M 33 with an error of 23%. Note that this method is a version of the rotational parallax method, but one that relies on external information [see § 4 and Olling & Peterson (2000)]. All the systematic effects that could affect the RP method are also important for the water-maser work, especially when only a limited number of sources are available per galaxy [M 31 is expected to have 17 H<sub>2</sub>O masers at *SKA* sensitivity (Brunthaler et al. 2006)]. When the *SKA* becomes operational, many more fainter maser sources will be detected in galaxies out to 100 Mpc (Fomalont 2005), while a distance accuracy of 1% can be achieved out to 30 Mpc (Fomalont & Reid 2004). At this distance, the perturbations in the Hubble flow would allow for a determination of about 10% per galaxy: the more distant sources would allow for the 1% goal on  $H_0$ .

Rather than averaging the proper motions per masing region, the H<sub>2</sub>O maser data can be utilized in a manner similar to their Galactic equivalents to derive distances. That is to say: a dynamical model of the star-forming region is used to predict the relation between the observable radial velocities and proper motions. Such models can either be based on ordered motions (such as rotation or expansion) or on isotropic random motions. See Argon et al. (2004) for a full description, references and an application to the IC 133 star-forming complex in M 33. For the case of the 14 year observing campaign of IC 133, Argon et al. (2004) adopt a random+systematic error of 22%, which is dominated by: 1) the unknown centre of expansion ( $\pm 16\%$ ), 2) random error ( $\pm 12\%$ ), and 3) an assumed expansion velocity (and error) of the group of maser spots (as determined by comparison with Galactic H<sub>2</sub>O masers;  $\pm 9\%$ ) and an assumed systemic velocity (and error) based on co-incident CO emission ( $\pm 4\%$ ). Although the expended effort is already enormous, it seems likely that the results could improve by at least a factor of two as a result of continued long-term monitoring (espe-

cially with the *SKA*), which would reduce the rms errors and would eliminate the secondary possibility for the expansion centre.

NGC 4258 is the current record holder for the most accurate extra-galactic distance, with a total error of about 5% as derived from the geometry and dynamics of its nuclear water maser sources (Herrnstein et al. 1999; Humphreys et al. 2005). The H<sub>2</sub>O masers are thought to arise in an almost edge-on circum-nuclear disk in Keplerian rotation. In this model, the masers occur close to the locations where the line-of-sight velocity gradients are small: that is to say, close to the major and minor axes of the velocity field (the major axis is also called the “midline”). Maser spots close to the major and minor axes are called the “high-velocity” and “systemic” masers, respectively. With the assumption of circular orbits, the observed positions and velocities can be converted to a model where the inclination ( $i$ ), the position angle ( $\phi$ ) and the rotation speed ( $V_c$ ) depend on radius ( $R$ ) only [see Herrnstein et al. (2005) and references therein]. Given this model, the distance can be derived in two independent ways from the systemic masers. First, the circular speeds of the systemic masers are directly observable as tangential proper motion with a value of about  $30 \mu\text{as yr}^{-1}$ . Because phase-referencing techniques are used to obtain the VLBA positions, absolute position information is lost (Herrnstein et al. 2005), so that the systemic proper motion of the galaxy is effectively subtracted from the observations. Thus, the above relations amount to a specialized version of the rotational parallax technique (see §4). The conversion from observed position to radial coordinate  $R$  introduces the largest systematic uncertainty in distance because  $V_c$ ,  $i$  and  $\phi$  change fairly rapidly with radius. The second technique employs the change in radial velocity ( $V_r$ ) that occurs due to the orbital motion of the systemic masers. In almost edge-on geometry and with  $V_c \sim 1100 \text{ km s}^{-1}$  and  $P$  about 750 yr, the accelerations are about  $9 \text{ km s}^{-1} \text{ yr}^{-1}$ . These two geometric techniques yield consistent results.

### 2.1.3 Nuclear Water Maser: Eccentric Orbits

A systematic uncertainty that has hitherto not been investigated is that of elliptical orbits in the masing region. It is well established that the majority of the high-luminosity cousins of NGC 4258 often exhibit significant degrees of non-axisymmetry in their disks (Strateva et al. 2003). Furthermore, models employing disks with substantial ellipticity were very successful in describing the observed optical double-peaked line profiles of AGN (Eracleous et al. 1995), who infer orbital eccentricities of order three-tenths. Such large eccentricities could result if the AGN contains in fact a binary black hole, or the tidal disruption of a normal star for the case of a single black hole. In such models, it seems likely that the water-masing region would also be affected because the radio emission is generated just a few times further out than the optical emission lines. However, other explanations exist for the optical emission lines, and it is not clear that elliptical orbits do in fact occur in accretion

disks (Storchi-Bergmann et al. 2003). In fact, models with such large and persistent eccentricities have been ruled out on the basis of long-term spectroscopic monitoring of several AGN (Gezari, Halpern & Eracleous 2007). Nevertheless, it seems that the possibility of elliptical orbits should be taken into account in the systematic-error budget of nuclear water masers, because eccentricities thirty times smaller than those ruled out by Gezari, Halpern & Eracleous (2007) would still bias the inferred distances (see below). Observations of other maser lines (if present) which probe different regions of the accretion disk would also minimize the uncertainty associated with large-scale non-circular motions.

Here we analyze a simple version of the general case of elliptical orbits where the major axis of the ellipse is aligned with the line of sight and show that this geometry yield observables that are indistinguishable from the case of circular orbits, albeit for a different distance, inclination and mass. For illustrative purposes we also assume that the disk is not warped. This case is worked out in some detail in Appendix A, where we find the following relation the distance [eqn. (A20)]:  $D_c/D_t = \sqrt{(1 \mp e)^3/(1 \pm e)} \approx 1 \mp 2e$ , where  $D_c$  is the distance that would be inferred under the assumption of circular orbits,  $D_t$  the true distance as derived for non-circular orbits, and where the minus (plus) signs correspond to case that the masing occurs at peri- (apo-) centre. Thus, if circular orbits are assumed but the orbits have in fact a small ellipticity, the true distance is smaller (larger) than the inferred distance by approximately twice the true orbital eccentricity if the systemic masers occur at peri- (apo-) centre. We have not investigated the case that the major axis is not aligned with the line of sight, but we surmise that a case will result intermediate between the peri- and apo-centre situations, so that the true distance will be uncertain by a factor of approximately  $(1 \pm 2e)$ .

#### 2.1.4 Light Echo Methods

“Light Echo” methods have been proposed and applied to the absorption of the super nova (SN) “pulse” by gas surrounding the progenitor, which is then re-emitted in the form of line radiation. This method has been applied to SN 1987A in the LMC by several authors [e.g., Panagia et al. (1991); Gould (1995); Gould & Uza (1998); Panagia (1999)], but it leads to a systematic (unresolvable) distance uncertainty of about 10% (Gould 2000). So far, this method has only been applied to SN 1987A.

Alternatively, one can attempt to use the polarized reflection of the SN pulse off dust in the circum-stellar material. The polarization condition strongly favors scattering by  $90^\circ$ , so that the physical radius equals the speed of light times the time-lag between the SN pulse and the detection of the polarized scattering event (Sparks 1994). If the proper motion of the light echo can be determined, the dependence on the assumed scattering angle is largely eliminated (Sparks 1996). Although previous searches for such events have not produced the hoped-for results (Boffi et al. 1999; Romaniello et al. 2005), current workers indicate that

the method works quite well (Sugerman, 2006, private communications).

A variant of the “pulse” method has recently been developed by Draine & Bond (2004). Their method employs strong X-ray sources behind nearby galaxies. The dust in the foreground galaxy scatters the X-rays to produce a halo around the source position. If the background source is variable, then intensity of this halo will vary with time and position, where the time-lag ( $\Delta t$ ) is directly related to the angular distance ( $\theta$ ) from the source and distance ( $D$ ) to the foreground galaxy:  $\Delta t \sim 140 D \theta_{100}^2$  days, with  $D$  in Mpc and  $\theta_{100}$  in units of 100 arcsec. For M 31 Draine & Bond (2004) estimate that a Chandra observing campaign of 5C 3.76 with a duration of 2 months (4 months) would yield a distance accuracy of 4% (1%). However, less observing time would be required if observing starts after an “outburst” of the background source. This method might also be applied if a gamma-ray burst would occur behind a nearby galaxy.

The “Expanding Photosphere” method can also be used to model the light curve and expansion history of supernovas. In this method the distance follows from the measured angular size and the physical size calculated from integration of the radial velocities. Mitchell et al. (2002) developed the “Spectral-fitting Expanding Atmosphere Method” which is specifically tailored to the time-varying and non-LTE nature of SN atmospheres (ejecta). This method has distance accuracies of order 10% and has been applied out to  $z=0.3$  (Nugent et al. 2006).

#### 2.1.5 Binary Star Methods

Detached Eclipsing Binaries (DEBs) are expected to be good distance indicators throughout the Local Group, possibly as good as 1% (Paczynski & Sasselov 1997; Paczynski 1997; Fitzpatrick et al. 2003; Wilson 2004). In this method, photometric observations of the eclipses determine the period, the flux ratio and the ratio of the stellar radii ( $R_*$ ) and the size of the orbit, while radial velocity observations determine the latter quantity directly. Spectroscopy and/or multi-band photometry can yield the effective temperature ( $T_{eff}$ ) of the stars. The absolute luminosity ( $L_*$ ) can be determined if the relation between surface brightness ( $F_*$ ) and  $T_{eff}$  is reliably determined, so that:  $L_* = 4\pi R_*^2 F_*$ . After correction for extinction, the observed brightness ( $F_{obs}$ ) then yields the distance:  $d = \sqrt{L_*/(4\pi F_{obs})} = R_* \sqrt{F_*/F_{obs}}$ . After 10 years of active research [e.g., Guinan et al. (1998); Kaluzny et al. (1998); Stanek et al. (1998); Ribas et al. (2002); Fitzpatrick et al. (2003); Ribas et al. (2004, 2005); Hilditch et al. (2005); Bonanos et al. (2006)], the best accuracies are currently about 5%. Possible reasons for the accuracy gap are the difficulty to determine the effective temperature, surface brightness and extinction. Also, the early-type main-sequence stars that are used in the DEB method have no local analogs with accurate distances and surface brightness measurements: none of the 150 *HIPPARCOS* stars earlier than B3 have a parallax better than 5%. We expect

that the *GAIA* data will provide the necessary calibration data (distances and extinction) to fully exploit the distance-scale potential of DEBs. Finally, DEBs are not ideal distance indicators: when using semi-detached systems or over-contact systems there are fewer (stellar) parameters to be solved for so that more accurate distances can be obtained [Wilson, 2002, private communications; Wyithe & Wilson (2002); Wilson (2004)].

A fundamental-physics method involving binary stars is via the detection of gravitational waves of close white dwarf binary (CWDB) stars with LISA. After 10 years of LISA operation, Cooray & Seto (2005) expect to be able to obtain a distance error for the LMC of order  $4.5\% \times \sqrt{N_{CWDB}/22}$ , where the expected number of CWDBs ( $N_{CWDB;exp} = 22$ ) may be uncertain by a factor of ten.

### 3 IMPLICATIONS FOR COSMOLOGY

There are at least four reasons to determine  $H_0$  with an *accuracy* of several percent or better: 1) to determine distances to external galaxies via redshift measurements, 2) to calibrate accurately other distance indicators, 3) to determine the equation of state of Dark Energy, and 4) to determine the total density ( $\Omega_{tot}$ ) of the universe. The equation of state (EOS) of Dark Energy (DE) tells us something about its nature.

Several lines of evidence suggest that we live in a Universe that is close to critical density ( $\Omega_{tot} \sim 1$ ). For example, the *WMAP* data and the *HST* constraint on the Hubble constant ( $h = 0.74 \pm 0.08$ ) results in  $\Omega_{tot} \sim 0.996$  and a mass density (baryons & dark matter) of 23%, so that about 76% of the energy-density of the universe is unrelated to gravitating matter. The most obvious candidate for this Dark Energy is a cosmological constant  $\Lambda$ , which is allowed for by General Relativity. Other forms of DE are suggested by theoretical physics. One difference between these various possibilities is the equation of state of the proposed DE candidates. For example, the cosmological constant would have  $w = -1$ , cosmic strings have  $w = -1/3$ , domain walls have  $w = -2/3$ , while Quintessence can come in multiple varieties: fixed with  $w \gtrsim -0.8$ , or with a time-variable  $w$  value (Peebles & Ratra 2003). We discuss two scenarios. In §§3.1 and §§3.2 we discuss the case of a constant  $w$ , while in §§3.5 we discuss the case of varying  $w$ , and compare our results with the recent conclusions of the Dark Energy Task Force (Albrecht et al. 2006).

Hu (2005; hereafter H05) analyzes in quite some detail how measurements of  $H_0$  and its variation with redshift would be beneficial for our understanding of dark energy and its evolution. He concludes that: "... the Hubble constant is the single most useful complement to CMB parameters for dark energy studies ... [if  $H_0$  is] ... accurate to the percent level ... ." However, Hu does not explicitly describes how errors on the dark-energy parameters are related to errors on  $H_0$ , while such information is of pre-eminent importance

when justifying and planning observational campaigns to determine  $H_0$ , especially if space missions are considered. In the remainder of this section, we present some analytical estimates for the relationship between the errors on  $H_0$  and the dark-energy parameters. These relations are approximate and are intended to facilitate estimating the required observing time (and cost) of observing programs aimed at determining  $H_0$ .

For the reader's convenience, we here present a short summary of Hu's (2005) description as to how CMB data physically relate to the Hubble constant. In fact, the CMB experiments determine the photon-to-baryon ratio ( $R_*$ ) and the matter-to-radiation ratio ( $r_*$ ) from the locations and ratios of the acoustic peaks. H05 finds:  $r_* \propto \frac{0.126}{\omega_m} \frac{1+z_*}{1089}$ , and  $R_* \propto \frac{\omega_b}{0.0223} \frac{1089}{1+z_*}$ , where  $\omega_b \equiv \Omega_b h^2$  is the physical baryon density. These relations allow us to derive the errors ( $\epsilon$ ) on  $R_*$  and  $r_*$  from the errors on  $\omega_m$  and  $\omega_b$  as given by WMAP07. The results are:  $\epsilon_{r_*} = 7.1\%$  and  $\epsilon_{R_*} = 3.6\%$  for  $\omega_m = 0.126 \pm 0.009$ , and  $100 \omega_b = 2.23 \pm 0.08$ . Physically, the co-moving size of acoustic oscillations ( $s_*$ ) equals the distance a sound wave has traveled during the time between the Big Bang and recombination, and depends on  $R_*$ ,  $r_*$ ,  $z_*$  and the sound speed (and hence the matter density  $\omega_m$ ):  $s_* \approx 139.8 \left(\frac{R_*}{0.854}\right)^{-0.252} \left(\frac{r_*}{0.338}\right)^{0.083}$  Mpc (scaled from H05), with a 1% uncertainty. Note that  $z_*$  depends only weakly on cosmology. The CMB data also yields the location of the acoustic peak ( $\ell_A$ ) with smaller error than that of  $s_*$ . Thus, the angular-diameter distance of the acoustic peak ( $D_A$ ) is well-established observationally:  $D_A \equiv \ell_A s_*/\pi$ , while theoretically  $D_A$  depends on cosmology:

$$D_A(\Omega_K = 0) = a_* \int_{a_*}^1 \frac{1}{a^2 H(a)} da \quad (1)$$

$$H(a) = H_0 \sqrt{\frac{\Omega_m}{a^3} + \frac{\Omega_\Lambda}{a^{3(1+w)}}} \quad (2)$$

where we neglect the small contribution from the density in relativistic particles ( $\Omega_\nu/a^4$ ), and where  $a = 1/(1+z)$  is the scale factor of the universe. If the curvature density ( $\Omega_K$ ) does not vanish, eqn. (1) needs to be modified [e.g., Carroll (2001)]. In this simple model, the sum of the  $\Omega$ -terms equals unity so that:

$$\Omega_\Lambda \equiv 1 - \Omega_m = 1 - \omega_m/h^2 \approx 0.770 \pm 0.022, \quad (3)$$

where the approximate value for eqn. (3) follows from the CMB value for  $\omega_m$  and the *HST* value for  $h$ . Thus, accurate determinations of  $\omega_m$  and  $h$  would significantly constrain the dark-energy. However, because the measured  $D_A$  is an integral constraint, it reveals nothing about the variation of  $H$  with scale-factor (or redshift or time). If in reality  $w$  varies with scale factor, while it is assumed to be constant, then application of the integral constraint would result in an erroneous value of  $H_0$  and/or  $w$ . However, if  $w$  is constant, as would be the case if the DE results from the cosmological constant, cosmic string, domain walls, etc., then a determination of  $H_0$  would nail down  $w$ . Be-

cause the variation of  $w$  is an important discriminator between various possible dark-energy candidates [see, e.g., Peebles & Ratra (2003); Flambaum (2006); Avelino et al. (2006); Albrecht et al. (2006), and references therein] one would want to determine the variation of  $w$  accurately.

### 3.1 A Flat Universe

Here we consider the case that the universe is flat, and if the equation of state is constant. For this simple case, we can determine the EOS of dark energy from the CBM data and the Hubble constant only. We use this example to illustrate that dark-energy information is contained in accurate knowledge of  $H_0$ . For the case of a flat universe ( $\Omega_K = 0$ ) and with  $\Omega_\nu = 0$ , eqn. (2) can be simplified to read:

$$\frac{\overline{H}(a)}{100} = \sqrt{\frac{\omega_m}{a^3} + \frac{h^2 - \omega_m}{a^{3(1+w)}}} \quad (4)$$

If the dark energy is in the form of a cosmological constant with  $w = -1$ , then the only unknown left in eqn. (4) is the Hubble constant which can be found from the constraint provided by the observed value of  $D_A$  [eqn. (1)]. From  $h$ ,  $\Omega_m$  and  $\Omega_\Lambda$  follow trivially. This is the basis for the reported determination of the Hubble constant from the *WMAP* data. However, the inferred value of the Hubble constant (and hence  $\Omega_m$  and  $\Omega_\Lambda$ ) depends on the choice of the EOS of the dark energy [via the  $1/a^{3(1+w)}$ -term in eqn. (4)]. This relationship is illustrated in Fig. 15 of *WMAP07*, from which we derive:

$$-w \approx 1.59 - 2.56 \Omega_m = 1.59 - 2.56 \frac{\omega_m}{h^2} \quad (5)$$

where the second equality is re-written in terms of the observables. The errors on the EOS and the density of dark energy for the case of a flat universe are thus:

$$\epsilon_{\Omega_\Lambda} = \Omega_m \sqrt{\left(\frac{\epsilon_{\omega_m}}{\omega_m}\right)^2 + \left(\frac{\epsilon_h}{h}\right)^2} \approx 2.8\% \quad (6)$$

$$\epsilon_w \approx 2.56 \Omega_m \sqrt{\left(\frac{\epsilon_{\omega_m}}{\omega_m}\right)^2 + \left(\frac{\epsilon_h}{h}\right)^2} \approx 7.2\% . \quad (7)$$

With uncertainties of 7.1% for  $\omega_m$  and 9.8% for  $h$  (including the systematic error term) the uncertainties on  $w$  and  $\Omega_\Lambda$  are almost evenly divided between the two error terms. However, in the future this will no longer be the case because the *PLANCK* mission is expected to reduce the error on  $\omega_m$  by a factor of eight (Efstathiou 2005). This indicates that in the post-*PLANCK* era, our knowledge of the value of dark energy will be fully dominated by the uncertainty on  $H_0$  if the (systematic) error on  $H_0$  is not decreased significantly, and if no other data is considered. Blake et al. (2004) reach a similar conclusion albeit that they argue that the CMB data imparts a correlation between  $\omega_b$  and  $\omega_m$  that will yield the same  $s_*$  so that it is impossible to go below  $\epsilon_w \sim 0.1$  employing  $H_0$  and CMB data alone. We note that this assertion is at odds with H05's who concludes that  $\omega_b$  and  $\omega_m$  are virtually independently determined from the CMD data.

### 3.2 Including Curvature

When adding other relevant data sets, the various cosmological parameters are determined better than with *WMAP* data alone. Inspecting Figure 21, Table 11 and Figure 17 of *WMAP07*, we derive the following  $\chi$ -by-eye relations for  $\Omega_\Lambda$ ,  $\Omega_K$  and  $w$ , respectively:

$$\Omega_\Lambda = a_{\Lambda m} + b_{\Lambda m} \Omega_m \quad (8)$$

$$\Omega_K = a_{K\Lambda} + b_{K\Lambda} \Omega_\Lambda \quad (9)$$

$$w = a_{wK} + b_{wK} \Omega_K . \quad (10)$$

We estimate the coefficients to equal:  $a_{\Lambda m} \sim 0.944 \pm 0.011$ ,  $b_{\Lambda m} \sim -0.775$  and  $a_{K\Lambda} \sim -0.0992 \pm 0.009$ ,  $b_{K\Lambda} \sim 0.1199 \pm 0.0124$  (the  $K\Lambda$ -terms are determined excluding the  $H_0$  constraint in Table 11 of *WMAP07*) and  $a_{wK} \sim -0.910 \pm 0.063$ ,  $b_{wK} \sim 6$ . In order to investigate the effects of the Hubble constant, we combine equations (8) through (10) in terms of  $h$  and arrive at:

$$\Omega_\Lambda = (0.944 \pm 0.011) - 0.775 \frac{\omega_m}{h^2} \quad (11)$$

$$\approx 0.766 \pm 0.020 \text{ (2.6\%)} \quad (11)$$

$$w = a_{wK} + a_{K\Lambda} b_{wK} + a_{\Lambda m} b_{K\Lambda} b_{wK} + b_{\Lambda m} b_{K\Lambda} b_{wK} \frac{\omega_m}{h^2} \quad (12)$$

$$= (-0.826 \pm 0.109) - (0.557 \pm 0.058) \frac{\omega_m}{h^2} \quad (13)$$

$$\approx -0.95 \pm 0.11 \text{ (11.6\%)} , \quad (13)$$

where the relations that are not numbered employ the values and errors on  $\omega_m$  from the CMB and  $h$  from *HST*. Comparing the relation for  $w$  for a flat universe [eqn. (5)] with the general case [eqn. (13)] we notice two things. First, the error is larger for the general case, presumably due to the extra degree of freedom that arises from fitting for  $\Omega_K$ . Second, the dependency on the value of  $H_0$  has decreased by a factor of almost five as evidenced by the smaller coefficient of the term containing  $h$ . This is probably due to the fact that the relations for the general case were derived employing the other data sets. Also note that  $\Omega_\Lambda^{flat}$  equals  $\Omega_\Lambda^{general}$  to within the errors, and that the derived errors are approximately the same for the two cases.

For the general case, we can now also obtain an expression for the total density:

$$\Omega_{noK} = \Omega_\Lambda + \Omega_m = a_{\Lambda m} + (b_{\Lambda m} + 1) \frac{\omega_m}{h^2} \quad (14)$$

$$= (0.9438 \pm 0.0114) + 0.225 \frac{\omega_m}{h^2} \quad (15)$$

$$\approx 0.996 \pm 0.016 \text{ (1.6\%)} . \quad (16)$$

Thus, without the assumption of a flat Universe, current data allows for the determination of the total density of the universe to plus or minus 1.6%, while the EOS of Dark Energy is known to about 12%. The actual values of  $\Omega_{tot}$  and  $w$  strongly hint at a flat Universe with the cosmological constant being the Dark Energy.

### 3.3 $H_0$ and Dark Energy

Future CMB data will be more accurate than at present: the eight-year *WMAP* data will reduce the current errors by a factor of two (Spergel, 2006, private communications), while *PLANCK* data is expected to be eight times better than the 3-year *WMAP* data (Efstathiou 2005).

We can estimate the effects of more accurate CMD data, as well as an accurate value of the Hubble constant on our knowledge of the EOS of Dark Energy by employing equation (12) above. In order to do so, we assume that the errors on the  $a_i$  and  $b_i$  parameters improve while the values themselves do not change with improved CMB accuracy. The advantage of this method is that it is easily implemented. A full, WMAP07-style, calculation could be performed, but is beyond the scope of this paper.

As discussed in §3, the physics of the CMB implies that only a *relation* can be found between  $\Omega_\Lambda$  and  $\Omega_m$ . This leads to a very elongated confidence region. Other data sets are required to break this degeneracy. For example, the magnitude-redshift relation for Supernova Ia is popular because its confidence region is almost perpendicular to that of the CMB data [for reviews, see among others, Carroll (2001); Lewis & Bridle (2002); Riess et al. (2004); Efstathiou (2005); Perlmutter (2005)]. In that case, the SN-Ia data “selects” part of the confidence region generated by the CMB data to determine *values* for  $\Omega_\Lambda$  and  $\Omega_m$ . However, it will hardly decrease the *error* in  $\Omega_\Lambda$  (for a given  $\Omega_m$ ) because the SN-Ia confidence region is very elongated in the  $\Omega_\Lambda$  direction. Thus, orthogonal constraints are the way to determine parameter *values*, while the shape and direction of the joint confidence region is set by the data set with the smallest errors. In the remainder of this paper we assume that the CMB measurements will be the most accurate data set, so that the relations between the cosmological parameters given by equations (8) through (12) and (14) are approximately valid. We will also investigate the consequences of relaxing this assumption.

The results are presented in figure 1, where the top panel shows  $\epsilon_w$  as a function of improvement of our knowledge of the CMB parameters, with respect to the *WMAP* 3-year data. The four lines are computed for Hubble constants with errors of 10.8%, 5.4%, 2.7% and 1.1%, from top to bottom. These errors correspond to improvements with respect to the current error by factors of 1, 2, 4 and 10, respectively. The corresponding errors on  $w$  that are attainable with *PLANCK*-like data are, 8.9%, 4.8%, 3.0% and 2.3%, respectively. These errors are computed via the standard error propagation relations for equation (12). The part of the error on  $w$  that can be attributed to uncertainty in  $H_0$  ( $\epsilon_{w,h}$ ) depends on the relative accuracy of the CMB parameters and  $H_0$ . Currently, the error on  $H_0$  hardly affects our knowledge of  $w$ . However, with decreasing errors on the CMB parameters, our ignorance of the Hubble constant becomes the dominant contribution to the total error on  $w$  ( $\epsilon_{w,tot}$ ). This is illustrated in the bottom panel of figure 1 which shows

$\epsilon_{w,h}/\epsilon_{w,tot}$  as a function of the accuracy of CMB data and the Hubble constant.

From figure 1 we infer that at *PLANCK* accuracy, the errors on  $w$  will have only slightly decreased with respect to the current value of 11.5%. However, the accuracy on the EOS of Dark Energy improves significantly when the error on  $H_0$  is decreased significantly. In section 3.5 below we estimate the effects of significant improvements in the quality of the other data sets and show that in those cases the effects of improved knowledge of  $H_0$  diminishes.

### 3.4 $H_0$ and $\Omega_{tot}$

The deviation from spatial flatness [ $(1 - \Omega_{tot}) \equiv \Omega_K$ ] follows from Equation (16):  $\Omega_K \sim 0.004 \pm 0.016$ . Thus, the spatial curvature is currently known to within a factor of four. We applied the same error-propagation methods for  $\Omega_{tot}$  as for  $w$  and find a behavior for the error on  $\Omega_{tot}$  very similar to  $\epsilon_w$ , but at approximately ten times lower level. Thus, a determination of the Hubble constant at the 1% level would decrease the error on the spatial curvature by a factor 16: from a factor four to one-in-four.

### 3.5 Comparison with the results from the Dark Energy Task Force

In their recent report, the Dark Energy Task Force [DETF; Albrecht et al. (2006)] presented recommendations as to how to increase our knowledge of dark energy, and in particular its evolution. As a starting point, they used the CMD data as expected to be delivered by *PLANCK* and added to that the expected improvements of a large variety of other proposed space-based and/or ground based investigations based on Baryon Acoustic Oscillations, Galaxy Clusters, Supernovae and Weak Lensing. The uncertainty on  $H_0$  used by the DETF corresponds to the current systematic  $H_0$  error as derived from the *HST* data (Freedman et al. 2001).

Our work presented above is based on the case of a fixed EOS of the dark energy, where we also assumed that any future increase in accuracy would be dominated by the *PLANCK* results, and that the accuracies of the other data sets would remain the same. In DETF-speak, we use “Stage I” accuracies for the other data sets and find  $\epsilon_w=8.9\%$ . From the models tabulated by the DETF, we infer  $\epsilon_w$  values of approximately 3.6%, 2.4% and 1.45% for the combined Stage II, Stage III and Stage IV data, respectively<sup>9</sup>. But note that these accuracies are only reached if all

<sup>9</sup> The DETF considered explicitly DE models with varying values of the EOS:  $w(a) = w_0 + (1 - a)w_a$ , with  $w_0$  the value at the current epoch and  $w_a$  the slope of the EOS versus scale-factor relation. For any fitted linear relation, there is point (the “pivot point”) where the total error is minimal. In this case,  $w_p = w_0 + (1 - a_p)w_a$ , and  $a_p$  scale factor of the pivot point. The DETF used a figure of merit (*FoM*) to evaluate the effectiveness of the other data sets. The *FoM* is essentially  $FoM = 1/(\epsilon_{w_p} \epsilon_{w_a})$ . For

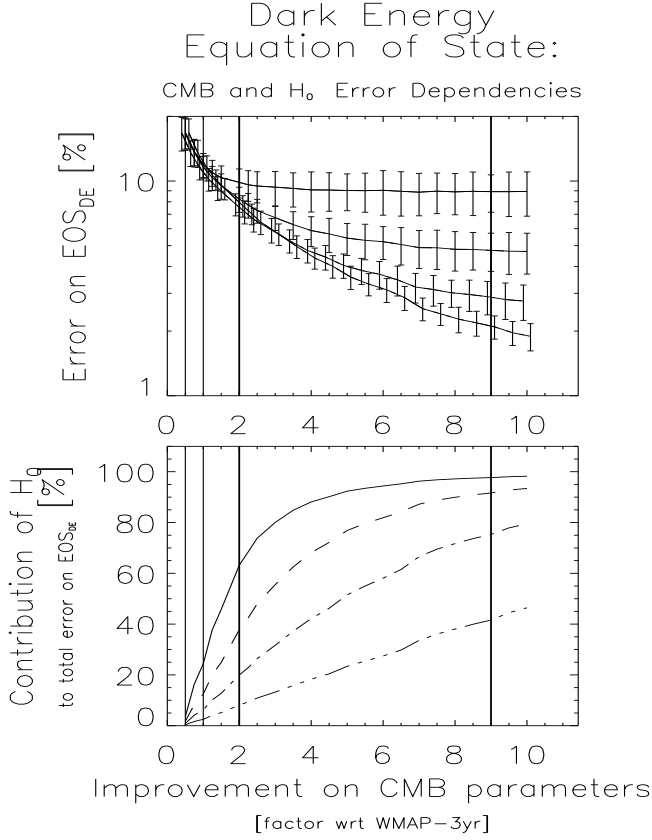


**Figure 1.** *Top Panel:* The accuracy with which the EOS of Dark Energy can be determined as a function of the accuracy of the CMB data (abscissa), and the accuracy in  $H_0$  (curved lines). The vertical lines correspond to accuracies of the *WMAP*-1-year data (left), *WMAP*-3yr data, *WMAP*-8yr data and *PLANCK* (right). With *PLANCK*-like CMB parameters and  $H_0$  accuracies of, from top to bottom, 10.8% ( $8 \text{ km s}^{-1} \text{ Mpc}^{-1}$ ), 5.4% ( $4 \text{ km s}^{-1} \text{ Mpc}^{-1}$ ), 2.7% ( $2 \text{ km s}^{-1} \text{ Mpc}^{-1}$ ) and 1.1% ( $0.8 \text{ km s}^{-1} \text{ Mpc}^{-1}$ ), the achievable errors on  $w$  are: 8.9%, 4.8%, 3.0% and 2.3%, respectively. The “error bars” represent the case that the slopes  $b_i$  in eqns. (8) – (10) are randomly varied by  $\pm 25\%$ . The lines in the *bottom panel* show the contribution of the uncertainty on  $H_0$  to the total error on  $w$  for  $\epsilon_{H_0}=8/1$ ,  $8/2$ ,  $8/4$  and  $8/10 \text{ km s}^{-1} \text{ Mpc}^{-1}$ , from top to bottom.

programs per stage are combined, and that all the programs in the previous stages are also executed.

Unfortunately, we can not directly compare our results with those of the DETF, but we can crudely scale our methodology to their results in the following manner. In our analysis, the strongest correlation (degeneracy) between parameters occurs for  $w$  and  $\Omega_K$ , with a coefficient of  $b_{wK} \sim 6$  [cf. eqn. (10)]. The effect of adding more accurate data is to break the degeneracies between the cosmological param-

models such as ours that do not include EOS evolution ( $w_a \equiv 0$ ), the “pivot point” lies at  $a_p = 1$ . We thus compare our  $\epsilon_w$  with  $\epsilon_{w_p}$  as tabulated by the DETF.

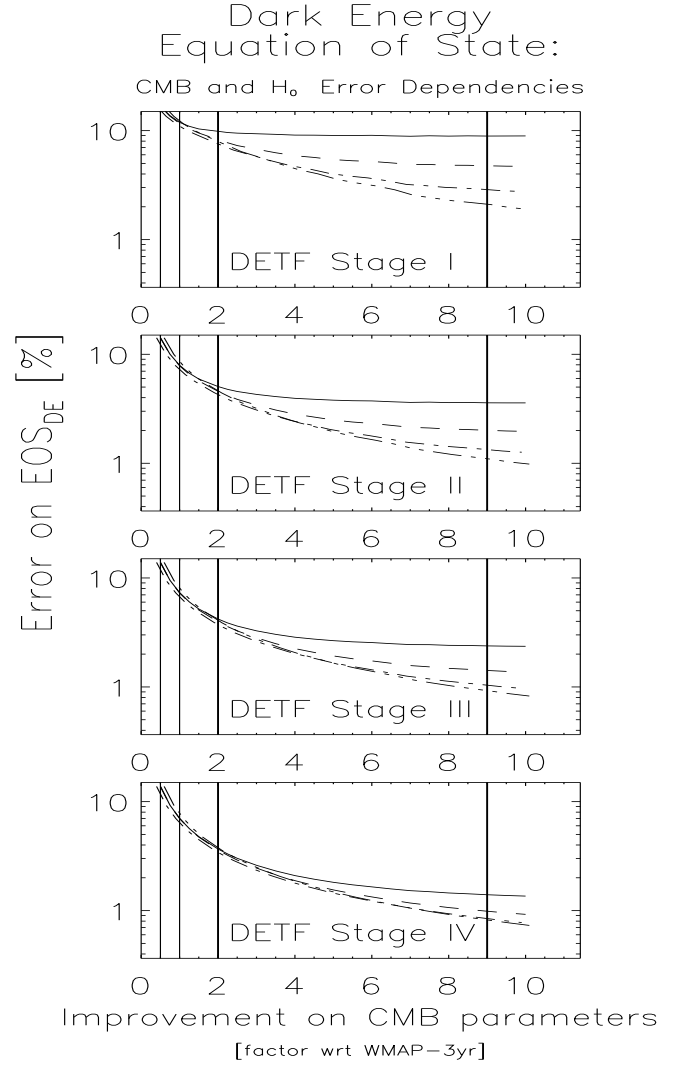


**Figure 2.** In each panel we present the accuracy with which the EOS of Dark Energy can be determined as a function of the accuracy of the CMB data (abscissa), and the accuracy in  $H_0$  (curved lines). The vertical lines correspond to accuracies of the *WMAP*-1-year data (left), *WMAP*-3yr data, *WMAP*-8yr data and *PLANCK* (right). The difference between the four panels is the accuracy with which the other data sets are determined. From top to bottom, these accuracies correspond approximately to stages I, II, III and IV as defined by the Dark Energy Task Force (see text, §§3.5), respectively. In each of the panels, the four lines correspond to the same errors on  $H_0$ :  $\epsilon_{H_0}=8/1$ ,  $8/2$ ,  $8/4$  and  $8/10 \text{ km s}^{-1} \text{ Mpc}^{-1}$ , from top to bottom. The attainable errors with *PLANCK* data are:  $\epsilon_w = 8.90\%$ ,  $4.81\%$ ,  $3.02\%$  and  $2.27\%$  for Stage I (as in Fig. 1;  $\epsilon_w = 3.60\%$ ,  $2.06\%$ ,  $1.43\%$  and  $1.20\%$  for Stage II;  $\epsilon_w = 2.41\%$ ,  $1.48\%$ ,  $1.14\%$  and  $1.02\%$  for Stage III;  $\epsilon_w = 1.45\%$ ,  $1.07\%$ ,  $0.95\%$  and  $0.91\%$  for Stage IV.

eters, which we implement by decreasing the value of  $b_{wK}$ . After some experimentation, we find that we recover the DETF  $\epsilon_w$  values if we decrease  $b_{wK}$  by factors of 2.51, 3.90 and 7.51 for Stages II, III and IV, respectively. The DETF tested the effects of smaller errors on  $H_0$  for Stage IV data, and conclude that a factor of two improvement would lead to a reduction of  $\epsilon_w$  by at most 50%, while we find an improvement of 26%, which is consistent with the DETF results.

Employing this calibration, we estimate the effects of smaller  $\epsilon_h$  values as a function of the accuracy of the other data. The results for Stages I, II, III and IV are presented in the top through bottom panels of Figure 2, respectively. Note that the top panel corresponds to our results discussed above (and Fig. 1), while the bottom panel corresponds to the best-case studied by the DETF. As expected, the effects of an improved error for  $H_0$  has less and less of an effect on  $\epsilon_w$  as the other data becomes more and more accurate.

Figure 2 suggests that some improvement in the other data sets can be traded for an improved error on  $H_0$ . That is to say, Stage I with  $\epsilon_h/20$ , Stage II with  $\epsilon_h/4$ , Stage III with  $\epsilon_h/2$  and Stage IV with  $\epsilon_h/1$  yield similar accuracies for the equation of state of dark energy. [We give the exact numerical results in the caption of Figure 2.] The DETF quotes that *each* of the Stage III projects would cost tens of millions of dollars (US), while the Stage IV projects might be as expensive as 300 – 1,000 M\$ *each*, or a total of at least 2,000 M\$. However, the primary motivations for each of these Stage IV projects are not necessarily related to dark-energy science. Nevertheless, we suggest that significant cost and time savings might be obtained if more effort is expended on determining a more accurate  $H_0$ , or at least that it would be worthwhile to investigate the matter more thoroughly. For example, a “VLBA” effort to find and analyze more extra-galactic water masers may reduce  $\epsilon_h$  by a factor of two to five at a cost of maybe several M\$, while a SIM-based rotational parallax program can reduce  $\epsilon_h$  by a factor of 5–10 and might cost 20 M\$. In fact, such a “VLBA” effort is already underway (Braatz *et al.* 2006).

#### 4 ROTATIONAL PARALLAX DISTANCES

The method of “Rotational Parallaxes” (RP) combines proper motions and radial velocities of stars in external galaxies to yield bias-free single-step distances, analogous to the orbital parallax technique. The attainable accuracies, of the order of one percent, are well matched to the requirement that the interpretation of future CMB data is not limited by knowledge on  $H_0$ .

For a nearby spiral galaxy at distance  $D$  (in Mpc) which is inclined by  $i$  degrees, with a rotation speed of  $V_c$  km s<sup>-1</sup>, the proper motion due to rotation equals  $\mu_{RC} = \frac{V_c}{\kappa D}$   $\mu\text{as yr}^{-1}$ , where  $\kappa \approx 4.74$  [kms<sup>-1</sup>]/[AU yr<sup>-1</sup>]. For M33 [ $i \sim 56^\circ$ ,  $D \sim 0.84$ ,  $V_c \sim 97$ ], M31 [ $i \sim 77^\circ$ ,  $D \sim 0.77$ ,  $V_c \sim 270$ ] and the LMC [ $i \sim 35^\circ$ ,  $D \sim 0.055$ ,  $V_c \sim 50$ ] we find:  $\mu_{RC}^{M33} \sim 24$ ,  $\mu_{RC}^{M31} \sim 74$  and  $\mu_{RC}^{LMC} \sim 192$   $\mu\text{as yr}^{-1}$ . Thus,

the rotational motions of these galaxies are easily resolved by *SIM*, and, depending on magnitude, also by *GAIA* and *OBSS*<sup>10</sup>. In addition to the absolute size of the rotation speed, the relative contribution of random motions of the stellar population ( $\sigma$ ) are important. The  $V_c/\sigma$  values of 27, 9.7 and 2.5 for M31, M33 and the LMC are likely to be indicative of the ease with which accurate RP distances can be determined.

The “principal axes” (or  $Mm$ ) variant of the RP method applies to galaxies dominated by circular rotation. Individual stars are identified along the major ( $M$ ) and minor ( $m$ ) axes at similar distances from the centre (with the same rotational velocity. Proper motions ( $\mu$ ) on the minor axis ( $\mu_m^C$ ) measure the circular velocity divided by  $D$ . On the major axis,  $\mu_M^C$ , equals  $\mu_m^C$  projected by  $\cos i$ . The correction for the systemic motion (indicated by superscript “C”) can be approximately achieved when *two* stars are chosen per principle axis, one on each side of the centre (e.g.,  $|\mu_M^C| = |\mu_{M,approaching} - \mu_{M,receding}|/2$ ). Radial velocities ( $V_r$ ) on the major axis give the circular velocity projected by  $\sin i$ . Combining these yields (Peterson & Shao 1997):

$$\cos i = \frac{|\mu_M^C|}{|\mu_m^C|} \quad (17)$$

$$V_c = \frac{V_r \mu_m^C}{\sqrt{(\mu_m^C)^2 - (\mu_M^C)^2}} \quad (18)$$

$$D_{Mm} = \frac{V_r}{\sqrt{(\mu_m^C)^2 - (\mu_M^C)^2}}. \quad (19)$$

However, the principal axes method requires stars close to the principal axes, making it difficult to find enough targets, while the effects of major perturbations such as warps, spiral arms etc. are difficult to handle.

This method can be generalized to a star arbitrarily positioned in the galaxy. We use rectangular ( $x$  and  $y$ ) and polar ( $R$  and  $\theta$ ) coordinate systems centred on the galaxy centre and co-planer with the galaxy disk. The  $x$  and  $y'$  axes along the major and minor axes, respectively, with  $y'$  is the foreshortened  $y$  coordinate. The following elementary relations between the coordinates and the various projections of the orbital velocity  $\bar{V}_c$  apply:

$$V_x = -s_\Omega V_c \sin \theta' \quad (20)$$

<sup>10</sup> We performed extensive simulations to convert accuracies in position or parallax to proper motion errors, with as a variable the inverse of the mission duration ( $x_t$ ). We find that  $\epsilon_\mu/\epsilon_{pos} \approx 1.901 x_t + 0.474 x_t^2$ , while  $\epsilon_\mu/\epsilon_\pi \approx 2.751 x_t + 0.981 x_t^2$ . Thus, for mission durations of 5 years, a position error at  $V=18$  of 5.38  $\mu\text{as}$  for *SIM* correspond to proper motion errors of 2.1  $\mu\text{as yr}^{-1}$ . *SIM*'s best grid accuracy is 3.47  $\mu\text{as}$  at  $V=11$ , so that  $\epsilon_\mu \sim 1.35$   $\mu\text{as yr}^{-1}$ . We estimate, based on *GAIA*'s scanning law, read noise, collecting area, quantum efficiency and integration time, that it can achieve parallax Eros of 26, 45 and 78  $\mu\text{as}$  at  $V=15$ , 16 and 17, respectively. This leads to proper motion errors of 15, 26 and 46  $\mu\text{as yr}^{-1}$ , at the same magnitudes.

$$V_y = s_\Omega V_c \cos \theta' = \frac{-V_x}{\tan \theta'} \quad (21)$$

$$V_r = V_y \sin i = s_\Omega V_c \cos \theta' \sin i \quad (22)$$

$$\mu_{y'} = \frac{V_{y'}}{\kappa D} = \frac{V_y \cos i}{\kappa D} = \frac{s_\Omega V_c \cos \theta' \cos i}{\kappa D} \quad (23)$$

$$\mu_x = \frac{V_x}{\kappa D} = \frac{-s_\Omega V_c \sin \theta'}{\kappa D}, \quad (24)$$

with  $V_x$  and  $V_y$  the projections of the  $\overline{V}_c$  vector on the  $x$  and  $y'$  axes. The angle  $\theta'$  is the angle between  $\overline{V}_c$  and  $V_y$ , while  $s_\Omega = -1$  (+1) for (counter-) clockwise rotation.

The three unknowns  $D$ ,  $i$  and  $V_c$  can be recovered from the three observables ( $V_r$ ,  $\mu_x$ , and  $\mu_{y'}$ ) by solving eqns. (22) – (24). Equations (25) – (27) below codify the “individual star” (*IS*) method:

$$D_{IS} = \frac{V_r}{\kappa} \sqrt{\frac{-y'/\mu_{y'}}{x\mu_x + y'\mu_{y'}}} \quad (25)$$

$$\cos^2 i_{IS} = \frac{y'\mu_{y'}}{-x\mu_x} \quad (26)$$

$$V_{c,IS} = V_r \sqrt{\frac{\mu_x}{\mu_{y'}} \frac{x\mu_{y'} - y'\mu_x}{x\mu_x + y'\mu_{y'}}}, \quad (27)$$

where we assume circular orbits.

The achievable distance error depends on distance, inclination, position angle and (almost) linearly on observing errors (OP2000). Evaluating eqn. (25) at various positions ( $x, y'$ ) in the target galaxy, and if we assume that the accuracies for the radial velocity observations ( $\epsilon V_r$ ) and proper motions are of order the internal velocity dispersion of the tracer population, we obtain a distance error (per star) of 13% for M31. For individual stars in M33 and the LMC, we get errors per star of 28% and 90%. Note that for M31 and M33 the random motions of a young population (10  $\text{km s}^{-1}$ ) corresponds roughly to the expected proper motion accuracy of *SIM* of 2.1  $\mu\text{as yr}^{-1}$  but is much smaller than *GAIA*'s and *OBSS*'s accuracies. For the LMC, the internal motions roughly equal the astrometric errors of *GAIA* and *OBSS*<sup>11</sup>. Also note that the distance error of 28% for M33 is quite close to the value obtained from H<sub>2</sub>O-masers method by Brunthaler et al. (2005).

Thus, for RP programs targeted at either M33 or M31, the main obstacle in achieving a small distance error is the smallness of the rotational signal. *SIM*, with its small errors, is thus much better suited for such a project. On the other hand, *SIM*'s small errors would be “wasted” on the LMC stars because there the error budget is dominated by the dispersion of the stellar population.

<sup>11</sup> For M31 and  $\sigma \sim 10 \text{ km s}^{-1} \sim \epsilon V_r$ , and  $\epsilon \mu \sim \sigma/(\kappa 770 \text{ kpc}) \sim 2.7 \mu\text{as yr}^{-1} \sim \epsilon \mu_{SIM} \ll \epsilon \mu_{GAIA}$ ,  
 – For M33 and  $\sigma \sim 10 \text{ km s}^{-1} \sim \epsilon V_r$ , and  $\epsilon \mu \sim \sigma/(\kappa 840 \text{ kpc}) \sim 2.5 \mu\text{as yr}^{-1} \sim \epsilon \mu_{SIM} \ll \epsilon \mu_{GAIA}$ ,  
 – For the LMC, the “errors” are dominated by the velocity dispersion ( $\sigma \sim 20 \text{ km s}^{-1}$ ) of the stars:  $\epsilon \mu \sim \sigma/(\kappa 55 \text{ kpc}) \sim 77 \mu\text{as yr}^{-1} \gg \epsilon \mu_{SIM} \sim \epsilon \mu_{GAIA}$

#### 4.1 Realistic Rotational Parallaxes

If not modeled carefully, non-circular motions due to spiral-arm streaming motions, perturbations from nearby galaxies, a bar, warps, etc. may result in a biased distance determination (OP2000). We have already seen that the obtainable errors for the idealized case of stellar-velocity-dispersion effects only yields errors of 13%, 28% and 90% for M31, M33 and the LMC, respectively. Since the errors due to random motions are stochastic, these errors would go down with the inverse of the square-root of the number of “stars” in the sample. In addition to the uncertainty due to velocity dispersion, spiral-arm streaming motions can reach amplitudes of 10% of the rotation velocity, leading to *systematic* distance errors of similar magnitude. For the LMC the effects of the bar and tidal interaction are even more important than for M31 and M33. In order to achieve errors of several percent, it will be necessary to correct for any sizable deviations from circular motion. OP2000 indicate that such can indeed be achieved with the next-generation astrometric satellites.

##### 4.1.1 Rotational Parallax: General Case

For the general case, we separate the three-dimensional motion of a star in four parts: 1) the systemic motion ( $\overline{V}_{sys}$ ) of the galaxy, 2) a random velocity  $\overline{V}_\sigma$ , 3) the circularly symmetric part of the orbital velocity  $\overline{V}_c$ , and 4) the peculiar component  $\overline{V}_p$ . The idea behind this separation is to group physical effects together that cause large-scale correlations between stellar motions that are amenable to modeling. The systemic and circular terms are easy to model, while the random term can only be taken into account in a statistical sense. The ease with which the peculiar velocity can be modeled depends on its cause. Thus, the total space motion of a star in an external galaxy is given by:

$$\overline{V}_{total} = \overline{V}_{sys} + \overline{V}_{orbit} + \overline{V}_\sigma, \text{ and where} \quad (28)$$

$$\overline{V}_{orbit} \equiv \overline{V}_c + \overline{V}_p. \quad (29)$$

Each term projects onto the orthogonal directions ( $\hat{x}, \hat{y}, \hat{z}$ ).  $\overline{V}_c$  corresponds to the rotation speed  $V_c$ , with components  $V_{c,x} = V_c \sin \theta$  and  $V_{c,y} = V_c \cos \theta$ , and  $\tan \theta = y/x$ . If the systemic motion makes an angle  $i_s$  with respect to the sky, the three observable velocities are:

$$\kappa D \mu_x = V_x = V_{sys,x} + V_{\sigma,x} + V_{c,x} + V_{p,x} \quad (30)$$

$$\kappa D \mu_{y'} = V_{y'} = V_{sys,ry'} \cos i_s + (V_{\sigma,z} + V_{p,z}) \sin i + (V_{c,y} + V_{p,y} + V_{\sigma,y}) \cos i \quad (31)$$

$$V_r = V_{sys,ry'} \sin i_s - (V_{\sigma,z} + V_{p,z}) \cos i + (V_{c,y} + V_{p,y} + V_{\sigma,y}) \sin i, \quad (32)$$

where  $V_{sys,ry'}$  is the component of the systemic motion in the plane spanned by the radial and minor axis directions. Note that the inclusion of the  $V_{sys}$  terms ensures that the velocity-gradient effects [Gould (2000); and § 2.1.1] are

taken into account self-consistently. These relations involve three observables ( $\mu_x$ ,  $\mu_{y'}$  and  $V_r$ ) and  $3 \times 3 + 4 = 13$  unknowns (3  $V_{sys}$  terms, 3  $V_\sigma$  projections, 3  $V_p$  terms,  $V_c$ , the azimuthal angle  $\theta$ , distance and inclination). Furthermore, all observables are expressed with respect to a coordinate system specified by four additional unknowns: galaxy centre  $(x_0, y_0)$ , position angle of the major axis ( $\phi$ ) and height ( $z$ ) above the midplane of the target galaxy<sup>12</sup>. Two more observables are available in the position  $(x, y')$  of the star. We end up with 5 observables and 17 unknowns<sup>13</sup>.

Obviously, this set of equations cannot be solved. However, substantial simplifications can be made when “averaging” over several stars. First, the velocity dispersion terms need not be determined for individual star but only for the group as a whole, so that only 14 unknowns remain (3 unknowns shared by all objects). Second, all stars share the same systemic motion, so that the  $V_{sys}$  terms follow from “averaging” suitably located objects (3 unknowns shared by all objects). Third, stars at similar distance from the galaxy centre share the same rotation speed, inclination, origin and orientation of the coordinate system (5 unknowns shared by all objects), and fourth, the distance is approximately constant<sup>14</sup> (1 unknown shared by all objects). Equations (30) – (32) can still not be solved because they involve five observables, five star-dependent unknowns ( $\bar{V}_p, \theta$ , and  $z$ ) and twelve shared unknowns ( $x_0, y_0, \phi, \bar{V}_\sigma, \bar{V}_{sys}, V_c, D$ , and  $i$ ).

To make progress, additional assumptions are needed to reduce the number of star-based unknowns. Several approaches are possible. In case A, once can assume that  $\bar{V}_p$  lies in the plane of the circular component as was done by OP2000. This assumption is justified if the perturbations arise from within the galaxy itself (*e.g.*, from the bar or spiral arms). Thus, in case A,  $V_{p,z} = 0$ , so that observations of  $N_A$  stars yield  $4N_A + 12$  unknown values and  $5N_A$  observables. In this case (A), the vertical position of each of the stars can be determined, as long as  $N_A \geq 12$ . Alternatively (case B), we can assume that, on average, the stars lie in the midplane ( $\langle z \rangle = 0$ ), so that observations of  $N_B$  stars yield  $4N_B + 12$  unknown values and  $5N_B$  observables. In this case (B), the full  $\bar{V}_p$  vector can be determined, as long as  $N_B \geq 12$ . Cases (A) and (B) can be generalized by employing simple parameterizations for either  $\bar{V}_p$  or the average mid-plane location  $\langle z \rangle$  as a function of azimuth. For example, the galaxy may exhibit some corrugation of

the plane [as in the Milky Way; *e.g.*, Levine et al. (2006), and references therein] in which case  $z$  may be expressed as a low-order Fourier series with  $N_{z,F}$  coefficients, which behave as shared variables. In the general case with  $N_{SV}$  shared variables and four star-based variables,  $N_*$  stars yield  $4N_* + N_{SV}$  unknowns and  $5N_*$  observables, leading to the requirement that:

$$N_* \geq N_{SV}. \quad (33)$$

Thus, observations of  $N_{SV}$  stars would suffice to determine four star-based parameters for each individual star, as well as the  $N_{SV}$  shared unknowns. Observing more objects will decrease the errors of the to-be determined parameters. Note that the equations of condition are mildly non-linear due to the trigonometric terms. However, good initial estimates are available for all shared unknowns, so that an unbiased solution should be attainable via iteration. This solution scheme is more robust than the simple method employed by Olling & Peterson (2000), and will be discussed in more detail elsewhere (Olling & Peterson 2007).

Employing the solution method outlined above, five of the six phase-space coordinates can be determined for each observed star. Such knowledge for a large number of stars is likely to be sufficient for the determination of non-circular motions, as well as the galaxy distance. As noted in the sections on extra-galactic water masers (§§ 2.1.2 and §§ 2.1.3), the water-maser method is limited by the fact that it samples only two lines of sight through the galaxy. On the other hand, the rotational parallax method is designed to map the galactic velocity field over a large range in azimuth with the explicit goal to be able to map out the non-circular motions. As a result, the RP method will yield more robust distances than the water-maser method, or, as a matter of fact, any other proposed method.

#### 4.1.2 Rotational Parallax: Observational Requirements

The distance errors can be reduced by observing more stars, if systematic errors in the data allow for such averaging. However, because non-circular motions can be correlated on large scales, a substantial number of stars needs to be used to be able to identify and correct for those systematic non-circular motions. Furthermore, these stars must be spread out over an area that exceeds the region affected by the non-circular motions. OP2000 envisaged using stars spread around an annulus in the target galaxy and estimated that a minimum of 200 stars are required to achieve a 1% distance error for M31. Thus, with *SIM* proper motions for about 200 stars per system, and if the non-circular motions can be handled properly, the distances to M31, M33 and the LMC can be determined to 0.92, 2.0 and 6.4 percent. The required *SIM* observing time for a rotational-parallax program depends on the magnitude of the stellar targets. For *GAIA*, with a fixed integration time per star, the final accuracy is determined by the total number of stars per target

<sup>12</sup> Although  $z$  does not appear explicitly in equations (30) – (32), it is present through the relation between the observable position  $y'$  and  $y$ :  $y' = y \cos i + z \sin i$

<sup>13</sup> We could add three more unknowns to handle any radial gradients in inclination, position angle and rotation speed.

<sup>14</sup> The nearby RP target galaxies are so close that they extend a substantial depth along the line of sight:  $\sim 7\%$ ,  $\sim 3.3\%$ , and  $\sim 2\%$ , for the LMC, M31, and M33, respectively. This problem is solved by replacing  $D$  by the sum of the distance to the system centre ( $D_{sys}$ ) and a position dependent distance:  $D = D_{sys} + d(x, y, z)$ . Note that this procedure does not add new unknowns, just more complexity.

galaxy, and the achieved astrometric accuracy as a function of magnitude.

If background galaxies and/or QSOs and stars internal to the Local Group galaxies can be measured simultaneously in the magnitude range 20 – 24 or so, a pointed, wide-field instrument such as *OBSS* or *TPF-C* might be well-suited to obtain the required astrometry. However, for a 1% distance estimate for M31 or M33, the imager needs to be stable to approximately  $\mu_{galaxy}/100\Delta t \sim 0.76\Delta t \mu\text{as}$ , or about  $3.8 \mu\text{as}$  for a five year mission ( $\Delta t = 5$ ). This amounts to about  $1/11,000^{\text{th}}$  of a pixel. The *HST* experience [ $1/100^{\text{th}}$  of a pixel] indicates that such accuracies would be hard to accomplish (Anderson & King 2003). Thus, an interferometer such as *SIM* is the natural instrument to use when very high accuracies are required. On the other hand, the large angular extent of the LG galaxies ensures that there are tens of thousands of usable background galaxies and many more galaxy-member stars, so that wide-field imagers might be able to the job.

By comparing on-galaxy star counts with off-galaxy counts on fields with the same Galactic latitude, we estimate that there are a sufficient number of potential targets in these three local group galaxies. Based on the UCAC2 catalog (Zacharias *et al.* 2004), we estimate that the LMC contains at least 23,000 stars brighter than  $V=16$  within two degrees from the centre. Similarly, the 2MASS catalog (Skrutskie *et al.* 2006) yields 2,009 ( $\pm 265$ ) and 984 ( $\pm 197$ ) stars with  $K_s \leq 15$  for M31 and M33, respectively. The LMC is a natural target for *GAIA*-based RP studies because, at the limiting magnitude of its radial velocity instrument ( $V \sim 17$ ), *GAIA*'s proper motion accuracy is smaller than the LMC's rotational signature of  $190 \mu\text{as yr}^{-1}$ .

Brunthaler *et al.* (2006) estimate the number of water masers in M31 to equal about 17 at an *SKA* sensitivity of 1 mJy. Applying their formalism, we expect a similar number water masers in M33. As we will show below, such small numbers of  $\text{H}_2\text{O}$  masers spread out over the disk of a galaxy are probably not very useful for the determination of unbiased distances at the percent level. Given the likely absence of tidal interactions in M33, we can probably use the case-A procedure of subsection 4.1.1 and neglect  $V_{p,z}$ . Because these masers will be spread out over the disk, the gradients parameters (for rotation speed, inclination and position angle) may also be important, so that the M33 case may require 15 shared variables, so that a minimum of 15 water masers are required [cf. equation (33)]. In such situations one might resort to using the results from the analysis of the neutral hydrogen (HI) emission (Corbelli & Schneider 1997). However, when employing those rotation-, inclination- and position-angle curves, the solution is no longer self-consistent. Furthermore, one may need to apply the velocity-gradient corrections [Gould (2000); and § 2.1.1] to interpret the HI data. In contrast, the large number of bright stars ( $\sim 1000$ ) makes M33 a natural target for *SIM*-based RP studies.

It has long been suspected that the interactions of

M32 and NGC205 cause spiral structure and warping in M31 [*e.g.*, Byrd (1978, 1983); Sofue & Kato (1981); Sato & Sawa (1986)]. Recent Spitzer data indicates that the so-called “ring of fire” (where most star formation occurs) is not centred on M31, and that the observed “split” in this ring is likely caused by a recent passage of M32 through M31's disk (Gordon *et al.* 2006). Given that most of M31's brightest stars (and hence water masers) are likely to reside in the ring of fire, and that the large-scale dynamics of these stars/masers may be significantly affected by tidal interaction, M31 may be a less suitable target for an RP program. Furthermore, the (expected) small number of water masers is probably not adequate for a reliable distance measure at the percent level. On the other hand, its large angular size makes M31 a natural candidate for stable, space-based wide-field imagers such as *OBSS*.

A successful dynamical model of the LMC would require at least all the ingredients uncovered by van der Marel *et al.* (2002), which include: 1) a time-dependent inclination, 2) an elliptical disk, 3) low rotation speed, 4) large internal velocity dispersion, 5) and a significant bar. In addition, the time-dependency of the position angle of the line of nodes needs to be considered. This model is thought to be sufficient to characterize the tidal effects of the Milky Way on the LMC. As such, the LMC may be a less favorable target for a rotational parallax program. Neglecting these perturbations, the minimum number of required stars (for a 1% distance) to overcome just the velocity-dispersion effects exceeds:  $N_{*,LMC} \geq (90\%/1\%)^2 = 8,100$ . However, given the much larger number of available bright stars, an accurate rotational parallax for the LMC might still be achievable with *GAIA*.

## 5 DISCUSSION AND CONCLUSIONS

In this paper we discussed a new, extremely accurate rung of the extra-galactic distance ladder, namely rotational-parallax method. Our preliminary analysis indicates that the best results might be obtained for the following galaxy/instrument(s) combinations: M33/*SIM*, M31/*SIM/OBSS* and LMC/*GAIA/OBSS*. In particular, we expect that the M33-*SIM* combination can obtain a bias-free distance with errors no larger than a percent or so. For M31/*SIM* the attainable accuracies are likely to be dominated by the degree to which the tidal distortions can be modeled. The results for galaxy/*OBSS*-combinations are limited by the level of systematics of the focal plane array. For the LMC/*GAIA* the main uncertainty is the degree by which localized errors can be beat-down by  $\sqrt{N}$  effects.

Assuming  $\sqrt{N}$  statistics for the Rotational Parallax method, 2% distance errors may be achieved with *SIM*-like observations of just 43 stars in M31 and 200 stars in M33. The LMC requires at least 2,025 stars to reach the desired distance accuracy, mainly because random motions are sig-

nificant, so that it is a preferred target for survey missions such as *GAIA*.

An accurate determination of the “first” rung of the extra-galactic distance ladder does not yield the Hubble constant. Distance indicators that extend well beyond the Local Group must be used for that. Thus, the RP method would enable a bias-free calibration of the secondary calibrators. On the other hand, the Water Maser Cosmology project (Braatz *et al.* 2006)

We expect that *GAIA*’s delivery of five-dimensional phase-space coordinates for a magnitude limited sample of individual stars of external galaxies (LMC, SMC et cetera) will have many significant galactic-dynamics applications such as bar-dynamics, disc dynamics and tidal interactions. On the other hand, M31 and M33 naturally lead to *SIM*-based programs because the internal motions (relative to the stellar velocity dispersions) are four to ten times smaller than for the LMC.

In this paper we focussed our cosmological analyses on the case that *PLANCK* data will be the norm for CMB data, and other data (Baryon Acoustic Oscillation, Galaxy Clusters, Supernovae and Weak Lensing) have accuracies at a level coined Stage I by the Dark Energy Task Force (Albrecht *et al.* 2006). In such a situation, the effects of decreasing the error on the Hubble constant on our knowledge of the equation of state of Dark Energy (and  $\Omega_{tot}$ ) declines when  $H_0$  is known more accurately. For example, with *PLANCK*-like CMB data, decreasing the error on  $H_0$  by a factor of two from the current uncertainty will almost half the error on  $w$ . However, when decreasing  $\epsilon_{H_0}$  from 2% to 1%,  $\epsilon_w$  (and  $\epsilon_{\Omega_{tot}}$ ) decreases by only 20% (see Fig. 1).

Scaling our analysis to the situation that the other data set are much more accurate than at present, we find that the effects of smaller  $\epsilon_{H_0}$  values become gradually less important. In accordance with the DETF we find that when the quality and quantity of the other data sets reaches the Stage IV level, decreasing  $\epsilon_{H_0}$  has only a minor effect.

An alternate utility of determining  $H_0$  with great accuracy from nearby galaxies is that it is fully independent of traditional cosmological analyses which *determine*  $H_0$ , while employing only a weak prior of its value. Especially when both methods yield  $H_0$  values with accuracies at the percent level or so, it becomes possible to test fundamental assumptions underlying CBM-type analyses such as the validity of general relativity as a description for the expansion of the Universe (Albrecht *et al.* 2006).

Other fundamental test of cosmology will become available via *SIM*, *GAIA* and *OBSS* astrometry in the form of determinations of very accurate ages of stars in (eclipsing) binary systems (Lebreton 2000). For such systems, all relevant fundamental stellar parameters (mass, radius, luminosity and metallicity) can be determined with great accuracy, leaving no wiggle room for stellar models. The accuracy of stellar dating is fundamentally limited by luminosity (distance) uncertainty because stellar evolution predicts luminosity ( $L$ ) evolution of about  $\Delta L/L \approx (0.24 -$

$0.106 \log \tau_{MS}) \pm 0.05$  per Gyr, where  $\tau_{MS}$  is the main-sequence (MS) lifetime of the star in Gyr [e.g., Olling (2003)]. A G6V star ( $0.89 M_{\odot}$ ) has a MS lifetime roughly equal to the age of the Universe, while its luminosity evolution amounts to about +12% per Gyr. If one-percent distances (2% in  $L$ ) are available for such stars in the Galactic halo, then a measurement of their apparent magnitude corresponds to a determination of their age to approximately  $1000 \times (2\%/12\%) = 166$  Myr. Such binary star observations will also yield the stars’ interior Helium abundance ( $Y$ ), so that  $Y(t)$  can be determined and extrapolated to  $t = 0$ . Many thousands of such halo stars are accessible by *GAIA*, *SIM* and *OBSS*, so that a very accurate lower limit of the age of the Universe can be obtained right here in the Solar neighbourhood. If one-percent distances are available for nearby Local Group systems, such accurate age determinations can potentially be made in those galaxies, so that a wide range in star-formation histories can be sampled.

I thank Dean Peterson, David Spergel, Ed Shaya and Alan Peel for useful discussions. I am also grateful for several suggestions by the referee to improve the paper.

## REFERENCES

- Albrecht, A., et al. 2006, astro-ph/0609591
- Alves, D. R. 2004, *NewAR*, 48, 659
- Alves, D. R., 2000, *ApJ*, 539, 732
- Anderson, J., & King, I. R. 2003, *PASP*, 115, 113
- Argon, A. L., Greenhill, L. J., Moran, J. M., Reid, M. J., Menten, K. M., & Inoue, M. 2004, *ApJ*, 615, 702
- Armstrong, J. T., et al. 1992, *AJ*, 104, 241
- Avelino, P. P., Martins, C. J. A. P., Nunes, N. J., & Olive, K. A. 2006, *PhRvD*, 74, 083508
- Bellazzini, M., Ferraro, F. R., Sollima, A., Pancino, E., & Origlia, L. 2004, *A&A*, 424, 199
- Bellazzini, M., Ferraro, F. R., & Pancino, E. 2001, *ApJ*, 556, 635
- Benedict, G. F., et al. 2006, Accepted to appear in the *Astronomical Journal*; astro-ph/0612465
- Benedict, G. F., et al. 2002, *AJ*, 124, 1695
- Blake, C. A., Abdalla, F. B., Bridle, S. L., & Rawlings, S. 2004, *New Astronomy Review*, 48, 1063
- Boffi, F. R., Sparks, W. B., & Macchetto, F. D. 1999, *A&AS*, 138, 253
- Bonanos, A. Z., et al. 2006, *Ap&SS*, 79
- Braatz, J., Greenhill, L., Condon, J., Henkel, Ch., Lo, F., Reid, M., 2006, the “Water Maser Cosmology Project” at:  
<http://www.cfa.harvard.edu/wmcp/index.html> and  
<http://www.cfa.harvard.edu/wmcp/talks/braatz.legacy.mtg.pdf>
- Brunthaler, A., Henkel, C., de Blok, W. J. G., Reid, M. J., Greenhill, L. J., & Falcke, H. 2006, *A&A*, accepted for publication & astro-ph/0606558
- Brunthaler, A., Reid, M. J., Falcke, H., Greenhill, L. J., & Henkel, C. 2005, *Science*, 307, 1440
- Byrd, G.G., 1983, *ApJ*, 264, 464
- Byrd, G.G., 1978, *ApJ*, 226, 70
- Carroll, S. M. 2001, *Living Reviews in Relativity*, 4, 1
- Cooray, A., & Seto, N. 2005, *ApJ*, 623, L113
- Corbelli E. & Schneider S.E., 1997, *ApJ*, 479, 244
- Da Costa, G. S., & Armandroff, T. E. 1990, *AJ*, 100, 162
- Davis, J., et al. 2005, *MNRAS*, 356, 1362
- Di Benedetto, G. P. 2002, *AJ*, 124, 1213
- Draine, B. T., & Bond, N. A. 2004, *ApJ*, 617, 987
- Durrell, P. R., Harris, W. E., & Pritchett, C. J. 2001, *AJ*, 121, 2557
- Edberg, S.J., Shao, M., Beichman, Ch.A. (editors),  
 SIM PlanetQuest, A Mission for Astrophysics and Planet-Finding  
[http://planetquest.jpl.nasa.gov/documents/WhitePaper05ver18\\_final.pdf](http://planetquest.jpl.nasa.gov/documents/WhitePaper05ver18_final.pdf)  
 or from: [http://planetquest.jpl.nasa.gov/SIM/sim\\_science\\_goals.cfm](http://planetquest.jpl.nasa.gov/SIM/sim_science_goals.cfm)
- Efstathiou, G., et. al, 2005, “The Planck Blue Book,” [www.rssd.esa.int/SA/PLANCK/docs/Bluebook-ESA-SCI\(2005\)1.pdf](http://www.rssd.esa.int/SA/PLANCK/docs/Bluebook-ESA-SCI(2005)1.pdf)
- Eracleous, M., Livio, M., Halpern, J. P., & Storchi-Bergmann, T. 1995, *ApJ*, 438, 610
- ESA, 1997, *The Hipparcos and Tycho Catalogues*, ESA Publication Division, ESTEC, Noordwijk, the Netherlands
- Feast, M., Catchpole, R.M., 1997, *MNRAS*, 286, L1
- Flambaum, V. V. 2006, *AIP Conf. Proc.* 869: Atomic Physics 20, 869, 29
- Fitzpatrick, E. L., Ribas, I., Guinan, E. F., Maloney, F. P., & Claret, A. 2003, *ApJ*, 587, 685
- Fomalont, E. B. 2005, *ASP Conf. Ser.* 338: Astrometry in the Age of the Next Generation of Large Telescopes, 338, 335
- Fomalont, E., & Reid, M. 2004, *New Astronomy Review*, 48, 1473
- Freedman, W. L., et al. 2001, *ApJ*, 553, 47
- Gezari, S., Halpern, J. P., & Eracleous, M. 2007, Accepted for publication in *ApJS* and astro-ph/0702594
- Gordon, K. D., et al. 2006, *ApJ*, 638, L87
- Gould, A., & Uza, O. 1998, *ApJ*, 494, 118
- Gould, A. 2000, *ApJ*, 528, 156
- Gould, A., 1995, *ApJ*, 452, 189
- Gould, A., 1994, *ApJ*, 426, 542
- Groenewegen, M. A. T. 2000, *A&A*, 363, 901
- Groenewegen, M.A.T., & Oudmaijer, R.D., 2000, *A&A*, 356, 849
- Groenewegen, M.A.T., et al., 2004, *A&A*, 420, 663
- Guinan, E. F., et al. 1998, *ApJ*, 509, L21
- Herrnstein, J. R., Moran, J. M., Greenhill, L. J., & Trotter, A. S. 2005, *ApJ*, 629, 719

- Herrnstein, J. R., et al. 1999, *Nature*, 400, 539
- Herrnstein, J. R., Greenhill, L. J., & Moran, J. M. 1996, *ApJ*, 468, L17
- Hilditch, R. W., Howarth, I. D., & Harries, T. J. 2005, *MNRAS*, 357, 304
- Hu, W. 2005, *ASP Conf. Ser.* 339: Observing Dark Energy, 339, 215
- Humphreys, E. M. L., Argon, A. L., Greenhill, L. J., Moran, J. M., & Reid, M. J. 2005, *ASP Conf. Ser.* 340: Future Directions in High Resolution Astronomy, 340, 466
- Johnston, K. J., et al. 2006, *PASP*, 118, 1428
- Kaluzny, J., Stanek, K. Z., Krockenberger, M., Sasselov, D. D., Tonry, J. L., & Mateo, M. 1998, *AJ*, 115, 1016
- Karachentsev, I. D., et al. 2006, *AJ*, 131, 1361
- Kervella, P., Bersier, D., Mourard, D., Nardetto, N., & Coudé du Foresto, V. 2004, *A&A*, 423, 327
- Kervella, P., Nardetto, N., Bersier, D., Mourard, D., & Coudé du Foresto, V. 2004, *A&A*, 416, 941
- Kennicutt, R.C., *et al.*, 2003, *A&A*, 202, 1114
- Kurucz, R. L. 2002, *ASSL Vol. 274: New Quests in Stellar Astrophysics: the Link Between Stars and Cosmology*, 3
- Lane, B. F., Creech-Eakman, M. J., & Nordgren, T. E. 2002, *ApJ*, 573, 330
- Lebreton, Y. 2000, *ARA&A*, 38, 35
- Lee, M. G., Freedman, W. L., & Madore, B. F. 1993, *ApJ*, 417, 553
- Levine, E. S., Blitz, L., & Heiles, C. 2006, *Science*, 312, 1773
- Lewis, A., & Bridle, S. 2002, *PhRvD*, 66, 103511
- Macri, L. M., Stanek, K. Z., Bersier, D., Greenhill, L., & Reid, M. 2006, 2006, *ApJ*, 652, 1133
- Madore, B.F., & Freedman, W.L., 1998, *ApJ*, 492, 110
- Madore, B. F., & Freedman, W. L. 1995, *AJ*, 109, 1645
- Makarov, D., Makarova, L., Rizzi, L., Tully, R. B., Dolphin, A. E., Sakai, S., & Shaya, E. J. 2006, *AJ*, 132, 2729
- Mitchell, R. C., Baron, E., Branch, D., Hauschildt, P. H., Nugent, P. E., Lundqvist, P., Blinnikov, S., & Pun, C. S. J. 2002, *ApJ*, 574, 293
- Mouhcine, M. 2006, *ApJ*, 652, 277
- Mouhcine, M., Rich, R. M., Ferguson, H. C., Brown, T. M., & Smith, T. E. 2005b, *ApJ*, 633, 828
- Mouhcine, M., Ferguson, H. C., Rich, R. M., Brown, T. M., & Smith, T. E. 2005, *ApJ*, 633, 810
- Newman, J. A., Ferrarese, L., Stetson, P. B., Maoz, E., Zepf, S. E., Davis, M., Freedman, W. L., & Madore, B. F. 2001, *ApJ*, 553, 562
- Ngeow, C., & Kanbur, S.M., 2006, *ApJ*, 642, L29
- Nordgren, T. E., Lane, B. F., Hindsley, R. B., & Kervella, P. 2002, *AJ*, 123, 3380
- Nugent, P., et al. 2006, *ApJ*, 645, 841
- Olling R.P., Peterson D.M., 2007, in preparation
- Olling, 2003, "Connecting the Physics of Stars, Galaxies and the Universe,"  
[http://www.astro.umd.edu/~olling/FAME/Astrometry\\_Stars\\_Galaxies\\_Universe.pdf](http://www.astro.umd.edu/~olling/FAME/Astrometry_Stars_Galaxies_Universe.pdf)
- Olling R.P., Peterson D.M., 2000, *astro-ph/0005484*
- Paczynski, B., 1997, in "The Extragalactic Distance Scale," ed. M. Livio, M. Donahue, & N. Panagia (Cambridge: Cambridge Univ. Press), p. 273
- Paczynski, B., & Sasselov, D. 1997, "Variables Stars and the Astrophysical Returns of the Microlensing Surveys;" Ed. by R. Ferlet, J-P. Maillard and B.e Raban, Cedex, France: Editions Frontieres, 1997., p.309
- Panagia, N., Gilmozzi, R., Macchetto, F., Adorf, H.-M., & Kirshner, R. P. 1991, *ApJ*, 380, L23
- Panagia, N. 1999, *IAU Symp.* 190: New Views of the Magellanic Clouds, 190, 549
- Peebles, P. J., & Ratra, B. 2003, *Reviews of Modern Physics*, 75, 559
- Perlmutter, S. 2005, *Physica Scripta Volume T*, 117, 17
- Perryman, M.A.C. *et al.* 2002, *ApSS*, 280, 1
- Peterson, D. & Shao, M. 1997, *ESA SP-402: Hipparcos - Venice '97*, 402, 749
- Iben, I., Jr., & Renzini, A. 1983, *ARA&A*, 21, 271
- Rizzi, L., Bresolin, F., Kudritzki, R.-P., Gieren, W., & Pietrzyński, G. 2006, *ApJ*, 638, 766
- Romaniello, M., Patat, F., Panagia, N., Sparks, W. B., Gilmozzi, R., & Spyromilio, J. 2005, *ApJ*, 629, 250
- Salaris, M., & Cassisi, S. 1997, *MNRAS*, 289, 406
- Sato, N.R., Sawa, T., 1986, *PASP*, 38, 63
- Skrutskie, M. F., et al. 2006, *AJ*, 131, 1163
- Sofue, Y. & Kato, T., 1981, *PASP*, 33, 449
- Sparks, W. B. 1996, *ApJ*, 470, 195
- Sparks, W. B. 1994, *ApJ*, 433, 19
- Reid, I. N. 1999, *ARA&A*, 37, 191

- Reid, M. J. 1993, *ARA&A*, 31, 345
- Ribas, I., Jordi, C., Vilardell, F., Fitzpatrick, E.L., Hilditch, R.W., Guinan, E. F. 2005, *ApJ*, 635, L37
- Ribas, I., Jordi, C., Vilardell, F., Giménez, Á., & Guinan, E. F. 2004, *New Astronomy Review*, 48, 755
- Riess, A. G., et al. 2004, *ApJ*, 607, 665
- Ribas, I., Fitzpatrick, E. L., Maloney, F. P., Guinan, E. F., & Udalski, A. 2002, *ApJ*, 574, 771
- Sandage A., *et al.*, 2006, astro-ph/0603647
- Sasselov, D.D., *et al.*, 1997, *A&A*, 324, 471
- Schilizzi, R. T. 2004, *Proceedings of the SPIE*, 5489, 62
- The SIM book, 1999 <http://sim.jpl.nasa.gov/library/book.html>
- Seljak, U., McDonald, P., & Makarov, A. 2003, *MNRAS*, 342, L79
- Soderblom, D. R., Nelan, E., Benedict, G. F., McArthur, B., Ramirez, I., Spiesman, W., & Jones, B. F. 2005, *AJ*, 129, 1616
- Spergel, D.N., *et al.*, 2003, *ApJS*, 148, 175
- Spergel, D.N., *et al.*, 2006, astro-ph, 063449
- Stanek, K. Z., Kaluzny, J., Krockenberger, M., Sasselov, D. D., Tonry, J. L., & Mateo, M. 1998, *AJ*, 115, 1894
- Storchi-Bergmann, T., et al. 2003, *ApJ*, 598, 956
- Strateva, I. V., et al. 2003, *AJ*, 126, 1720
- van der Marel, R. P., Alves, D. R., Hardy, E., & Suntzeff, N. B. 2002, *AJ*, 124, 2639
- White, M. 2006, *New Astronomy Review*, 50, 938
- Wyithe, J. S. B., & Wilson, R. E. 2002, *ApJ*, 571, 293
- Wilson, R.E., 2004, *NAR*, 48, 695
- Zacharias, N., *et al.* 2004, *AJ*, 127, 3043

**APPENDIX A: WATER MASERS & ELLIPTICAL ORBITS**

For the general case of elliptical orbits, Newtonian gravity and a dominant central object, the orbital speed at distance  $R$  is given by:

$$V_o(R) = \sqrt{\frac{GM_o}{a_o} \frac{2-\alpha}{\alpha}} \quad (\text{A1})$$

$$V_{o;km/s}(R) = 2\pi\kappa \sqrt{\frac{M_o}{a_{o;AU}} \frac{2-\alpha}{\alpha}} \quad (\text{A2})$$

where  $G$  is the gravitational constant,  $M_o$  the mass of the central object,  $a_o$  the semi-major axis of the orbit, and  $\alpha = R/a_o$ . The subscripts “c,” “e,” and “o” to indicate cases that are valid for circular, elliptical and general orbits. We also specify the units of the parameter in the subscript. For eqn. (A2) we express the velocity in  $\text{km s}^{-1}$ , with the mass of the central object always in units of  $M_\odot$ ,  $\kappa$  ( $\sim 4.74$ ) converts velocities in  $\text{AU yr}^{-1}$  to  $\text{km s}^{-1}$  and  $a_{o;AU}$  equals  $a_o$  in astronomical units. For circular orbits ( $\alpha = 1$ ), eqn. (A1) reduces to the well-known  $V_o(R) = \sqrt{GM/a_o}$ , while for orbits with eccentricity  $e$  at we have  $V_{o;peri} = \sqrt{GM/a_o \times (1+e)/(1-e)}$  at peri-centre and  $V_{o;apo} = \sqrt{GM/a_o \times (1-e)/(1+e)}$  at apo-centre.

For our test geometry (see §§ 2.1.3), the high-velocity masers are located at the tangent of the ellipse at distance  $R_{HV} = \sqrt{b^2 + (e a_e)^2} = \sqrt{(1-e^2)a_e^2 + (e a_e)^2} = a_e$  from the centre, where  $b$  is the semi-minor axis of the ellipse. Thus, for the high-velocity masers,  $\alpha$  equals unity, so that their observed radial velocities map out a rotation curve that is identical to the case of circular orbits.

To derive the expected kinematics, we use a coordinate system with  $x$  and  $y'$  axes that are aligned with the apparent major and minor axes (neglecting the position-angle warp), and with  $y$  the corresponding coordinate in the plane of the circum-nuclear disk (i.e.,  $y' = y \cos i$ ). Because the maser spots move only a small amount in azimuth during a multi-year experiment, we can approximate the orbital motion as being locally sinusoidal with constant angular velocity, and with period  $P_e \approx 2\pi R_e/V_e$ . Then, for Heliocentric distance  $D$ , the positions, radial velocities ( $V_r$ ), radial acceleration ( $\dot{V}_r$ ) and proper motion ( $\mu$ ) are:

$$x \approx R_o \sin\left(\frac{2\pi t}{P_o}\right) = R_o \sin\left(\frac{t V_o}{R_o}\right) \quad (\text{A3})$$

$$y \approx R_o \cos\left(\frac{t V_o}{R_o}\right) \quad (\text{A4})$$

$$\frac{V_{r,HV;o}}{\sin i_{HV;o}} = \dot{y}_{HV} = V_{HV;o} \quad (\text{A5})$$

$$\frac{|V_{r,S;o}|}{\sin i_{S;o}} = \dot{y}_{S;o} = V_{S;o} \sin\left(\frac{t V_{S;o}}{R_{S;o}}\right) \approx \frac{V_{S;o}^2}{R_{S;o}} t \quad (\text{A6})$$

$$\frac{|\dot{V}_{r,S;o}|}{\sin i_{S;o}} = \ddot{y}_{S;o} = \frac{V_{S;o}^2}{R_{S;o}} \cos\left(\frac{t V_{S;o}}{R_{S;o}}\right) \approx \frac{V_{S;o}^2}{R_{S;o}} \quad (\text{A7})$$

$$\mu_{S;o} = \frac{\dot{y}_{S;o}}{\kappa D} \approx \frac{V_{S;o}}{\kappa D_{S;o}}, \quad (\text{A8})$$

where we use the additional subscripts “S” and “HV” to indicate whether the expression is valid for the systemic or high-velocity masers, respectively. The units of the proper motion are  $\text{mas yr}^{-1}$  if the velocities are in  $\text{km s}^{-1}$  and the distance in kpc.

First, we will examine the constraints that derive from the high-velocity maser spots. For our toy model, the velocities in eqns. (A2) and (A5) are equal so that the observable radial velocity is:

$$V_{r,HV;o} = 2\pi\kappa \sin i_{HV;o} \sqrt{\frac{M_o 1000 D_{o;Mpc}}{a_{HV;o;mas}}}, \quad (\text{A9})$$

where  $a_{HV;o;mas}$  is the observed major-axis position of the high-velocity spot. Bringing all the observables to the left-hand side (LHS) yields:

$$\frac{a_{HV;o;mas} V_{r,HV;o}^2}{4000\pi^2 \kappa^2} = \sin^2 i_{HV;o} M_o D_{o;Mpc}, \quad (\text{A10})$$

where all the observables and all the unknowns are on the LHS and the right-hand side (RHS).

Turning our attention to the systemic masers, we use the observed minor-axis position of the systemic maser spots to determine an expression for the semi-major axis. First, we have:  $y_{S;o;AU} = R_{S;o;AU} \cos i_{S;o} = a_{o;AU} (1 - e_o) \cos i_{S;o} = y'_{S;o;mas} \times (1000 D_{o;Mpc})$ , so that:

$$a_{S;o;AU} = \frac{y'_{S;o;mas} \times (1000 D_{o;Mpc})}{(1 - e_o) \cos i_{S;o}} \quad (\text{A11})$$

$$\frac{a_{S;o;mas}}{y'_{S;o;mas}} = \frac{1}{(1 - e_o) \cos i_{S;o}}. \quad (\text{A12})$$

where the second relation has all observables on the LHS. Inserting eqn. (A11) into (A2) and the result into (A8), we find:

$$\frac{10^9}{4\pi^2} y'_{S;o;mas} \times \mu_{S;o;mas/yr}^2 = \frac{M_o \cos i_{S;o} (1 + e_o)}{D_{o;Mpc}^3}. \quad (\text{A13})$$

Further information is contained in the observed acceleration of the systemic maser spots: inserting eqn. (A2) evaluated at peri-centre into eqn. (A7) and using (A11) we obtain:

$$\frac{\dot{V}_{r,S;o} (1000 y'_{S;o;mas})^2}{4\pi \kappa^2} = \frac{\sin i_{S;o} \cos^2 i_{S;o} M_o (1 + e_o)}{D_{o;Mpc}^2}, \quad (\text{A14})$$

If one assumes circular orbits, a constant inclination and that  $a_S = a_{HV}$ , then there are two sets of three equations [[(A10), (A12) and (A13)] and [(A10), (A12) and (A14)]] that can be used to solve for the three unknowns: distance, inclination and the mass of the central object. If a simple warped model [ $i = i_0 + \beta(R - R_0)$ ] is adopted, one can determine the slope ( $\beta$ ) from the high-velocity maser spots because they have a warped (projected) geometry and a small non-Keplerian behavior (Herrnstein et al. 1996).

Equations (A10), (A12), (A13) and (A14) can be rearranged into the following relations between the circular and eccentric cases:

$$\sin i_{HV;c} \sqrt{M_c D_{c;Mpc}} = \sin i_{HV;e} \sqrt{M_e D_{e;Mpc}} \quad (\text{A15})$$

$$\cos i_{S;c} = (1 - e) \cos i_{S;e} \quad (\text{A16})$$

$$\frac{M_c \cos i_{S;c}}{D_{c;Mpc}^3} = \frac{M_e \cos i_{S;e} (1 + e)}{D_{e;Mpc}^3} \quad (\text{A17})$$

$$\frac{\sin i_{S;c} \cos^2 i_{S;c} M_c}{D_{c;Mpc}^2} = \frac{\sin i_{S;e} \cos^2 i_{S;e} M_e (1 + e)}{D_{e;Mpc}^2}, \quad (\text{A18})$$

where constraint equations (A15) – (A18) also equal the LH sides of equations (A10), (A12), (A13) and (A14), respectively. Again we can include a fifth relation from the warping behavior, but for illustrative purposes we will assume a constant inclination, so that we have four equations [(A15) – (A18)] with four unknowns [ $D$ ,  $i$ ,  $M$  and  $e$ ]. Expressing the first three unknowns as a function of the fourth, we find:

$$\frac{\cos i_e}{\cos i_c} = \frac{1}{1 - e} \approx 1 + e + 2e^2 + \mathcal{O}(e^3) \quad (\text{A19})$$

$$\frac{D_e}{D_c} = \sqrt{\frac{1 + e}{(1 - e)^3}} \approx 1 + 2e + \frac{5}{2}e^2 + \mathcal{O}(e^3) \quad (\text{A20})$$

$$\frac{M_e}{M_c} = \sqrt{\frac{1 + e}{(1 - e)^7}} \approx 1 + 4e + \frac{19}{2}e^2 + \mathcal{O}(e^3), \quad (\text{A21})$$

where the additional subscript “ $p$ ” indicates that these relations hold for systemic masers at peri-centre. One should keep in mind that eqns. (A19) – (A21) were derived for the special geometry described in §§ 2.1.3. These simplifications were used to illustrate the effects of unmodeled eccentric orbits for nuclear water masers, not to provide accurate relations for any specific case.

Above we have worked out the case that the systemic masing occurs at peri-centre. For the alternate case (masing at apo-centre), we find that we can replace  $e$  with  $-e$  in equations (A11) – (A21), including the approximations of (A19) – (A21).